REVIEWS

Journal of Semiconductors
(2021) 42, 031101
doi: 10.1088/1674-4926/42/3/031101

Indium–gallium–zinc–oxide thin-film transistors: Materials, devices, and applications

Ying Zhu, Yongli He, Shanshan Jiang, Li Zhu, Chunsheng Chen, and Qing Wan†

School of Electronic Science & Engineering, Nanjing University, Nanjing 210023, China

Abstract: Since the invention of amorphous indium–gallium–zinc–oxide (IGZO) based thin-film transistors (TFTs) by Hideo Hosono in 2004, investigations on the topic of IGZO TFTs have been rapidly expanded thanks to their high electrical performance, large-area uniformity, and low processing temperature. This article reviews the recent progress and major trends in the field of IGZO-based TFTs. After a brief introduction of the history of IGZO and the main advantages of IGZO-based TFTs, an overview of IGZO materials and IGZO-based TFTs is given. In this part, IGZO material electron travelling orbitals and deposition methods are introduced, and the specific device structures and electrical performance are also presented. Afterwards, the recent advances of IGZO-based TFT applications are summarized, including flat panel display drivers, novel sensors, and emerging neuromorphic systems. In particular, the realization of flexible electronic systems is discussed. The last part of this review consists of the conclusions and gives an outlook over the field with a prediction for the future.

Key words: indium–gallium–zinc–oxide; thin-film transistors; flat panel displays; sensors; flexible electronics; neuromorphic systems

Citation: Y Zhu, Y L He, S S Jiang, L Zhu, C S Chen, and Q Wan, Indium–gallium–zinc–oxide thin-film transistors: Materials, devices, and applications[J]. *J. Semicond.*, 2021, 42(3), 031101. http://doi.org/10.1088/1674-4926/42/3/031101

1. Introduction

Metal oxide semiconductor thin-film transistors (TFTs), especially indium–gallium–zinc–oxide (IGZO)-based TFTs, have received considerable interest since Nomura *et al.* reported the first amorphous IGZO (a-IGZO) based TFT in 2004. Before the invention of the first a-IGZO-based TFT, the crystalline IGZO materials were first reported as early as 1985[1]. However, it was not until 2003 and 2004 that Nomura *et al.* used the IGZO materials of single-crystalline and amorphous states as the TFT semiconductor channel materials, respectively[2, 3]. The key advantage of single-crystalline is that there are no defects or grain boundaries, which makes TFTs with ultra-high mobility. However, a high temperature is needed for single crystal growth, which is not favorable for large-area application. In 2004, Nomura *et al.* reported that a-IGZO film can be deposited at low temperature. Now, a-IGZO films have become the most common TFT channel semiconductor materials. Compared to amorphous silicon TFTs with a field-effect mobility lower than 1.0 $cm^2/(V{\cdot}s)$, a-IGZO-based TFTs usually show a field-effect mobility higher than 10 $cm^2/(V{\cdot}s)$[4–7].

Several well-known display companies (e.g., Sharp, Samsung Electronics, and LG Electronics) have demonstrated that IGZO-based TFTs have many potential applications in liquid crystal displays (LCDs), organic light emitting diodes (OLEDs) display and electronic paper displays[7–14]. In addition to flat panel displays, IGZO-based TFTs are also actively involved in sensor applications and neuromorphic systems. IGZO-based TFTs have the key advantages of distinguishable sensitivities to light, pressure, pH, gas, and some other parameters, which meet the requirements of these sensors. Furthermore, based on the relatively mature display technology, sensors with IGZO-based TFTs are easier to manufacture[15–30]. In particular, the IGZO-based TFTs show great potential in the field of flexible electronics because of their unique advantages of lightweight, ultrathin thickness and resistance to mechanical bending[13, 31–33]. IGZO-based TFTs with electrolyte gate dielectrics are very favorable for artificial synapse/neuron emulation, due to the interfacial electric-double-layer coupling and electrochemical doping effects[34–41]. IGZO-based TFTs neuromorphic devices show very low-energy consumption down to pJ/spike because of the extremely high gate capacitance of the electrolyte gate dielectrics and the high resistance of IGZO channel layers[42–45]. Some important applications of IGZO-based TFTs are shown in Fig. 1.

With the rapid development of IGZO-based TFTs in various aspects of our life, especially in the field of display, a large number of studies based on the IGZO-based TFTs have been reported. Thus, this article aims to review the recent progress and the major trends in the field of IGZO-based TFTs. In this paper, we review the materials, devices and applications of IGZO-based TFTs. First, the history, electron travelling orbitals and deposition methods of the IGZO thin film are introduced. Second, we introduce the traditional devices and the new-concept device structures. Third, we comprehensively discuss the main applications, including display drivers, sensor applications and neuromorphic systems using IGZO-based TFTs. Finally, our conclusions and the outlook for IGZO-based TFTs are discussed.

2. IGZO materials and TFTs

2.1. IGZO materials

Crystalline IGZO materials were first discovered by Kimi-

Correspondence to: Q Wan, wanqing@nju.edu.cn
Received 7 AUGUST 2020; Revised 12 OCTOBER 2020.

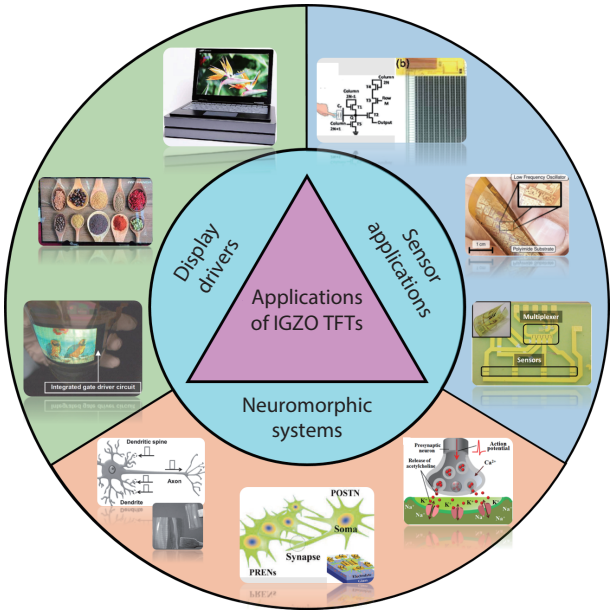

Fig. 1. (Color online) Some important applications of IGZO-based TFTs[11, 20, 34–37, 46–48].

zuka *et al.* in 1985[1]. These authors successfully fabricated $InGaZnO_4$ with $YbFe_2O_4$-type structure by sintering at a temperature above 1000 °C. Until 2003 and 2004, the single-crystalline and amorphous state IGZO materials were proposed for TFT channel semiconductors by Nomura *et al.*[2, 3], respectively. In 2003, Nomura *et al.* presented a transparent TFT with single-crystalline IGZO thin film as the channel layer. The unique advantages of the single-crystalline $InGaO_3(ZnO)_5$ thin film are that there are no grain boundaries and defects, which enable the single-crystalline IGZO-based TFT to show a field-effect mobility (μ_{FE}) as high as ~80 $cm^2/(V{\cdot}s)$. However, a high annealing temperature of 1400 °C was needed to form the single-crystalline phase. This high temperature process limited the practical application. In the next year, amorphous IGZO (a-IGZO) thin films were deposited at low temperature by Nomura *et al.*[3]. This a-IGZO thin film was prepared by pulsed laser deposition (PLD) using a polycrystalline $InGaZnO_4$ ceramic target. The first a-IGZO-based TFT showed a saturation mobility of 6–9 $cm^2/(V{\cdot}s)$, a current on/off ratio (I_{on}/I_{off}) of 10^3 and threshold voltage (V_{th}) of 1.6 V.

The electron travelling orbitals of oxide semiconductors are different from covalent semiconductors. Covalent semiconductors (e.g., silicon) possess carrier transport paths of directive sp^3 orbitals[3]. Thus, the electron mobility of single crystal silicon can reach up to 1000 $cm^2/(V{\cdot}s)$[38]. However, if the carrier conducting pathway was disrupted in the case that the crystalline structure was broken or under amorphous state, then the carrier mobility would be lower by three orders of magnitude than single crystal silicon[39]. Unlike covalent semiconductors, oxide semiconductors are of degenerate band conduction. Fig. 2 shows the carrier transport paths of crystalline and amorphous oxide semiconductors. The carrier transport paths of metal oxide semiconductors are composed of spatial metal n*s* orbitals with isotropic shape. Because *s* orbital is of spherical symmetric, the overlap in distorted metal–oxygen–metal can also offer a conductor pathway.

Many methods have been proposed to deposit IGZO thin films. The most commonly used method is sputtering because it is compatible with uniform deposition on the large surface with low cost[40, 41, 49]. Pulsed laser deposition (PLD)[3], atomic layer deposition(ALD)[50–52], plasma enhanced chemical vapor deposition (PECVD)[53–55] and solution methods such as spin-coating, inkjet printing and gravure printing[56] are also used for IGZO-based TFT fabrication. These methods possess unique advantages, for example, IGZO thin film grown by ALD showed a roughness at the atomic level. The PECVD method can well control the reactive species concentration and further regulate the film deposition rate.

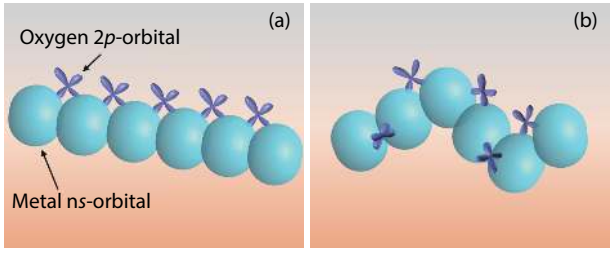

Fig. 2. (Color online) Carrier transport paths of (a) crystalline, (b) amorphous post-transition-metal oxide semiconductors[3].

2.2. IGZO-based TFTs

The first concept of thin-film transistors (TFTs) was patented as early as the 1930s[57]. However, TFTs were only at the concept stage without vacuum technology and an understanding of semiconductors. The first practical TFT was fabricated in 1962 by Weimer[58]. In his experiment, microcrystalline cadmium sulfide film was used as the semiconducting channel layer and silicon oxide was used as the gate dielectric. Since 2003, zinc oxide (ZnO) TFTs have attracted much interest[59–61]. However, ZnO films crystallize at low temperature and usually show polycrystalline structure, which is not suitable for large-area macroelectronics. Fortunately, Nomura *et al.* invented the first a-IGZO-based TFT in 2004[3]. IGZO-based TFTs have gradually gained practical applications thanks to their high electrical performance, large-area uniformity, and low processing temperature. Fig. 3 shows a time axis diagram of the development of the IGZO-based TFTs.

Many possible device structures for IGZO-based TFTs are shown in Fig. 4[63, 64]. Figs. 4(a)–4(e) show the bottom-gate structure, top-gate structure, dual-gate structure, vertical structure and multiple gate structure, respectively. Figs. 4(a) and 4(b) are the simplest device structures that require very few manufacturing steps, which are very friendly to the laboratory device preparation. For example, the structure in Fig. 4(a) just needs one lithographic step, which makes the device preparation relatively quick and cheap. However, the electrical properties of those devices are unstable because the channel materials are exposed to the atmosphere, and will be influenced by the moisture and oxygen in the air. In the dual-gate structure, just as the name implies, bottom gate and top gate are together used to control the device properties, such as the threshold voltage, subthreshold swing, current on/off ratio[65–68]. The devices of vertical structure possess small footprint, resistance to the bending stress and controllable channel length[69–71]. TFTs of multiple in-plane gate electrodes are used in neuro-transistors to simulate spatiotemporal information processing[72].

In IGZO-based TFTs, source/drain electrodes, gate elec-

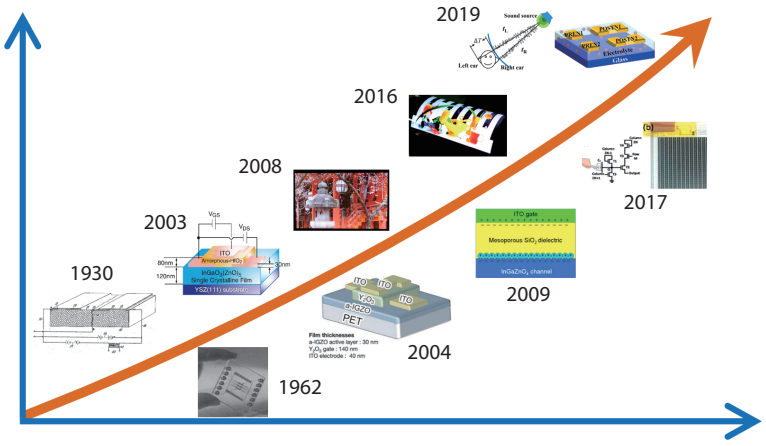

Fig. 3. (Color online) A time axis diagram of the development of the IGZO-based TFT[1–3, 11, 20, 36, 44, 57, 62].

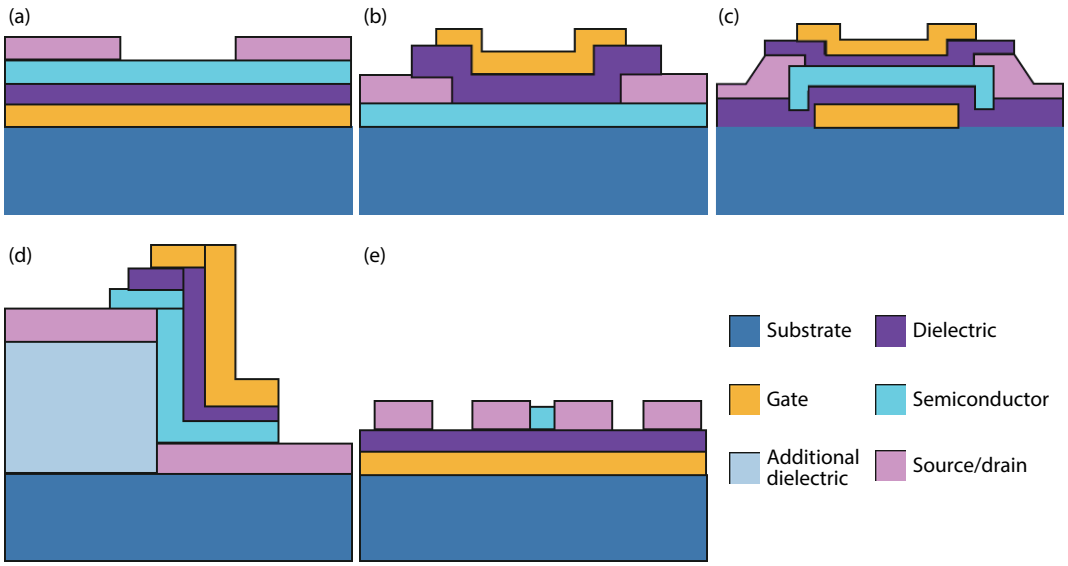

Fig. 4. (Color online) Schematic diagrams of the device structures with (a) bottom gate, (b) top gate, (c) double gate, (d) vertical and (e) multiple gates.

trode, gate dielectric and IGZO semiconductor channel material are used in the TFT structures. Electrodes are usually composed of metal materials, high conductive metal oxides and new materials such as graphene[70, 73, 74]. Various materials are used as gate dielectrics. First, traditional gate dielectrics like SiO_2 and SiO_x[66, 75], which can be compatible with traditional TFT fabrication process. Second, high κ materials, such as Al_2O_3, HfO_2, ZrO_2, Y_2O_3 and Ta_2O_5[50, 70, 76]. The advantages of these materials are that they can reduce the equivalent oxide thickness and decrease the device size. However, they are of poor interface quality and reduce compatibility with the TFT fabrication process. Third, organic gate dielectrics such as olefin polymers and polyvinyl pyrrolidone (PVP)[77, 78]. These organic gate dielectrics are usually used in the flexible electrics. Finally, ion gate dielectrics, such as proton conducting nanogranular SiO_2 and chitosan[79, 80]. These dielectrics are actively used in the electric-double-layer TFTs and produce a large capacitance.

Sato *et al.* presented a bottom-gate type coplanar homojunction a-IGZO-based TFT[75]. In this work, they employed highly doped contact regions naturally formed by depositing upper protection layers made of hydrogenated silicon nitride. As a result, a nearly ideal Ohmic contact was formed with a low parasitic source-to-drain resistance of 34 Ω·cm. Fig. 5(a) shows a schematic diagram of the TFT structure. The device was fabricated on a glass substrate. The molybdenum (Mo) layer was sputtered as the bottom-gate electrode. The SiO_x layer was deposited by PECVD as the gate dielectric. This gate dielectric material is commonly used because it is compatible with the traditional TFT fabrication process. Then, the a-IGZO semiconductor film was deposited by direct-current magnetron sputtering and used as channel layer at room temperature. SiO_x/SiN_x layer was deposited by PECVD and used as a protection layer. The region that was not covered SiO_x after depositing SiO_x/SiN_x film was converted to highly conductive source/drain electrodes. Figs. 5(b) and 5(c) show the transfer and output curves of the TFTs, respectively. The device showed a good subthreshold swing (SS) of 0.13 V/decade, a V_{th} of 0.13 V, and an I_{on}/I_{off} of over 10^9 at V_{ds} = 10 V. From the output characteristics, we can see a steep rise in the low V_{ds} region, which indicated a good Ohmic contact between semiconductive a-IGZO and source/drain electrode.

Zhang *et al.* proposed a self-aligned top-gate a-IGZO-based TFT with a thickness of 8.62 nm SiO_2 as gate dielec-

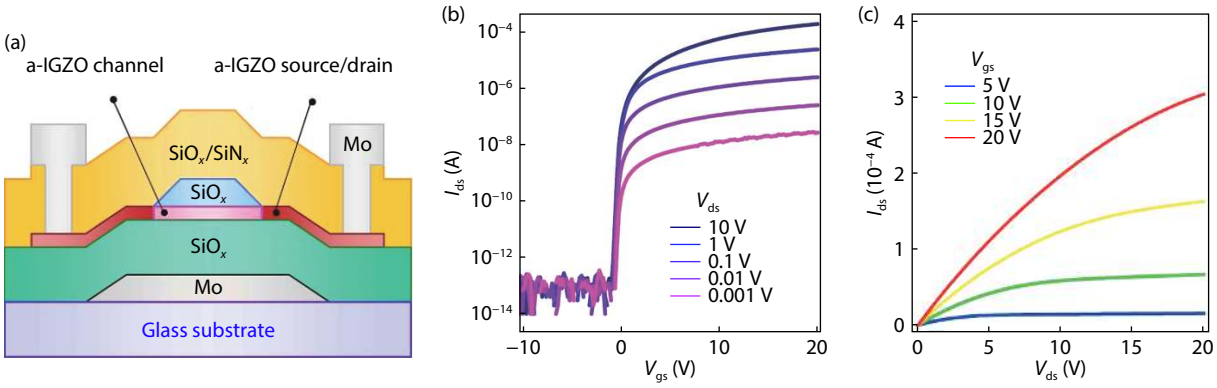

Fig. 5. (Color online) (a) Schematic diagram of the bottom-gate coplanar homojunction a-IGZO device structure. (b, c) Transfer and output curves of the device, respectively[75].

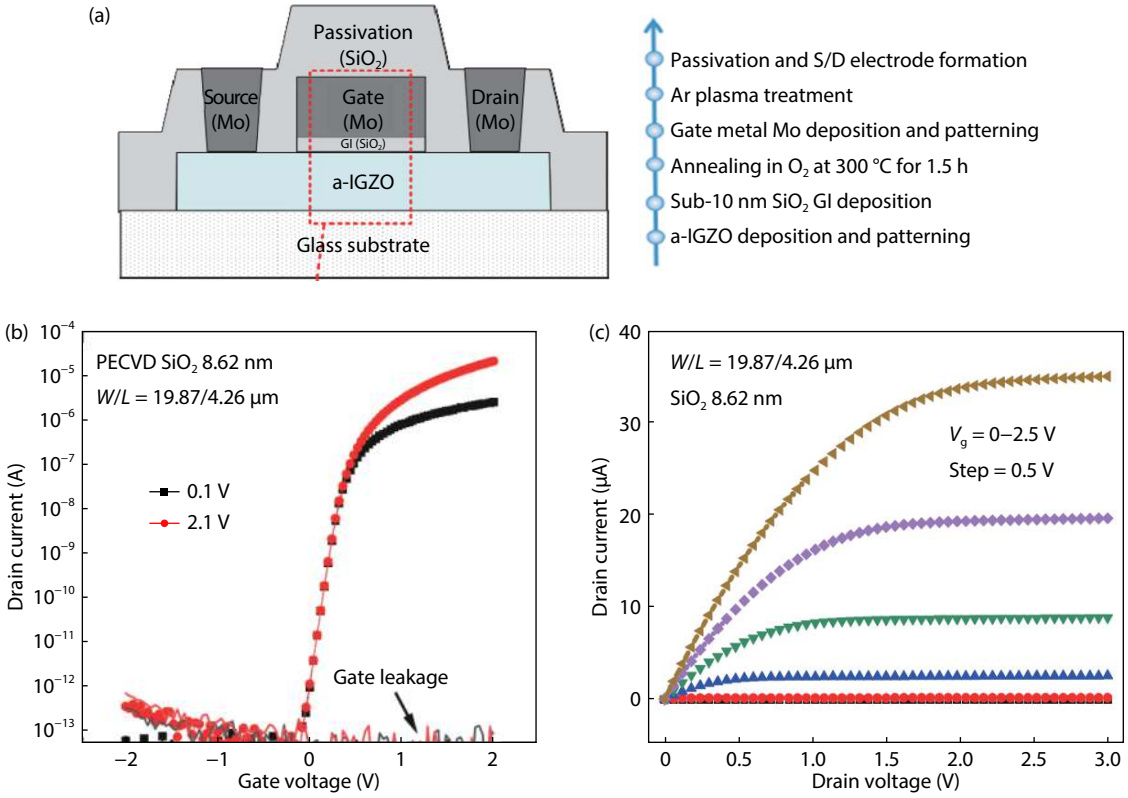

Fig. 6. (Color online) (a) Schematic diagram of the top-gate a-IGZO-based TFT structure and the major processing steps, respectively. (c, d) Transfer and output curves of the a-IGZO-based TFT, respectively[74].

tric[74]. This device realized the ultrathin gate dielectric less than 10 nm with low leakage current. Fig. 6(a) shows the structure of the TFT and the major processing steps, respectively. A thickness of 40 nm a-IGZO thin film was deposited on the glass substrate by sputtering at room temperature. A thin SiO_2 film with thickness lower than 10 nm was deposited as the gate dielectric by PECVD at 300 °C. The 80 nm thick Mo film was then deposited on the SiO_2 layer and patterned to form the gate electrode by dry etching. Finally, the Mo layer was used as the source/drain electrodes by a lift-off process. Figs. 6(b) and 6(c) show the transfer and output characteristics of the a-IGZO-based TFT, respectively. The a-IGZO-based TFT showed a low off-state current of less than 10^{-12} A, a low gate leakage current of 10^{-13} A, a μ_{FE} of 10.13 $cm^2/(V{\cdot}s)$, a V_{th} of 0.52 V and a high I_{on}/I_{off} over 10^8 at V_{ds} = 2.1 V. Such a-IGZO TFTs with ultrathin SiO_2 gate dielectric have achieved a low gate leakage current and have also shown a good electrical stability under positive and negative gate bias stresses.

In the dual-gate structure, the top gate and bottom gate are together used to modulate the channel carrier concentration and further control the electrical performance of the device, such as the turn-on voltage, the threshold voltage and the field-effect mobility, through applying voltage to the bottom and top-gate electrodes[81–84]. The work principle of dual-gate TFT is somewhat like that of the single-gate TFT, utilizing the electric field capacitively to control the channel. By changing the polarity or amplitude of the voltage applied to the bottom or the top gate, the channel actually becomes enhanced or depleted. The concentration of the conductive carriers (the majority carriers) changes and the electrical performance of the device can also be modulated. Li *et al.* presented a comparison between the single-gate and dual-gate TFTs[66].

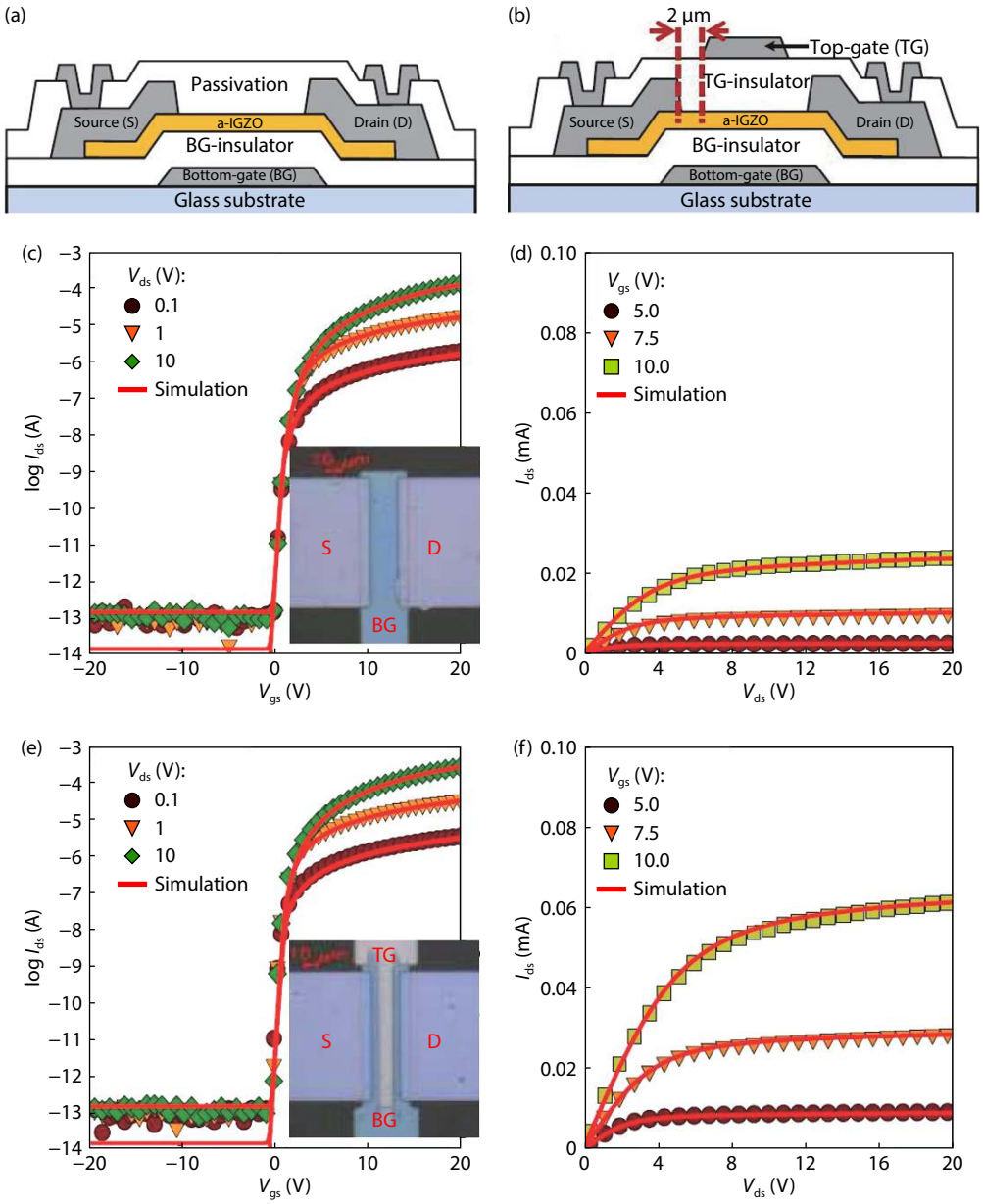

Fig. 7. (Color online) Schematic diagrams of the structures of (a) single-gate and (b) dual-gate TFT, respectively. (c, d) Transfer and output curves of the single-gate device, respectively. (e, f) Transfer and output curves of the dual-gate device, respectively[66].

Figs. 7(a) and 7(b) show the schematic structures of the single-gate and dual-gate devices, respectively. The a-IGZO thin film was deposited as the channel layer by reactive sputtering. Figs. 7(c) and 7(d) show the transfer and output curves of the single-gate TFT, respectively. Figs. 7(e) and 7(f) show the transfer and output curves of the dual-gate TFT, respectively. Compared with the single-gate TFT, the performance of the dual-gate TFT is more superior. The on current was 2.54 times higher than that of the single-gate TFT, the μ_{FE} was about 1.23 times higher than that of the single-gate TFT, and SS was about half of the single-gate TFT.

Vertical structure devices can offer ultrashort channel with high current. Furthermore, the ultrashort channel enables the device to resist mechanical stress, which is especially important for flexible devices[70]. In planar IGZO-based TFTs, a few cracks in the IGZO thin film can severely degrade the migration of the carriers. However, in vertical structures, the vertical current is unaffected by planar cracks. When the device suffers an external mechanical stress, usually causing several cracks across the IGZO thin film, as shown in Fig. 8(d), the TFTs in the vertical structure are less affected because the current transfer between the source and drain is in the vertical direction. Liu *et al.* presented a highly flexible vertical TFT with the IGZO thin film as the channel layer[70]. Fig. 8 shows the vertical device structure and the charge transport paths in the planar and vertical TFTs, respectively. The structure of the vertical TFTs is based on the vertical heterostructure of graphene-IGZO-metal stack. Tanium (Ti) was sputtered as the drain electrode. The IGZO thin film was deposited as the channel layer. The chemical vapor deposition (CVD) graphene was transferred onto the IGZO thin film as the source electrode. A thickness of 40 nm Al_2O_3 thin film was deposited on the top of the channel as the gate dielectric with high dielectric constant. When the cracks appeared in the IGZO thin film, as shown in Figs. 8(c) and 8(d), the carriers cannot be transported in the planar structure because the source/drain electrodes are both in the same plane and the current is blocked by the cracks. However, as shown in Figs. 8(a) and 8(b), the sou-

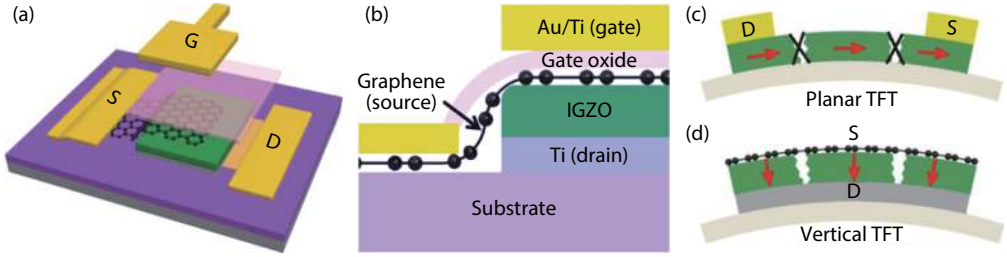

Fig. 8. (Color online) (a, b) Schematic diagrams of the vertical IGZO-based TFT structures. (c, d) Carriers transferred in the planar and vertical TFTs with cracks in the IGZO thin film, respectively[70].

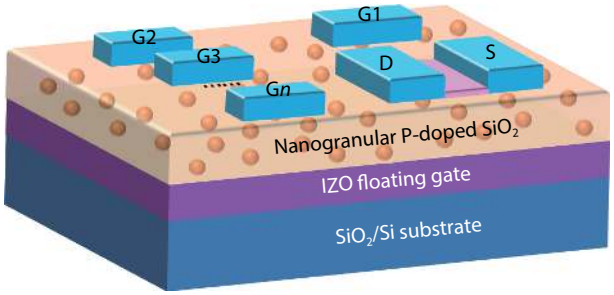

Fig. 9. (Color online) Schematic diagram of the IGZO-based neuron TFTs with multi-gate structure[72].

rce/drain electrode and gate electrode are in the vertical direction, and thus the carrier transfer are less affected. Based on the characteristics of the resistance to mechanical stress, these vertical structure TFTs are significantly favorable for the application of flexible electronics.

In 2017, IGZO-based neuron TFTs with multiple in-plane gate electrodes were reported by our group[72]. Fig. 9 shows the device structure of the neuron TFTs gated by a nanogranular SiO_2 electrolyte film. Electric-double-layer effect due to the mobile proton in the SiO_2 electrolyte film provided a very large specific gate capacitance. Voltage pulses applied on the in-plane gate electrodes can be temporally and spatially coupled to the IGZO channel layer due to the indium–zinc–oxide (IZO) floating gate. These IGZO-based neuron TFTs are favorable for sensors and neuromorphic applications.

3. Applications

IGZO-based TFTs have been applied in many areas, such as display drivers, sensors and neuromorphic systems[10, 23, 25, 85–88]. In this section, we will introduce the important applications based on IGZO-based TFTs in commercial production and scientific research.

3.1. Display drivers

Hydrogenated amorphous silicon (a-Si:H) and low-temperature polysilicon (LTPS) have been widely used in practical displays. However, the electron mobility of a-Si:H is usually low (1.0 $cm^2/(V{\cdot}s)$) and the TFTs are unstable under stress and illumination[4]. LTPS TFTs possess high mobility and good stability compared to a-Si:H TFTs[11]. Nevertheless, the process cost of preparing LTPS films is relatively high, especially for large-size displays[4, 5, 85, 89]. In addition to these two materials, the IGZO thin film has the advantages of high electron mobility, low-temperature fabrication process, high uniformity of large area and low cost. These advantages ensure that the IGZO-based TFTs are favorable for the applications of displays[9, 11–13, 31, 41, 85, 90–103].

3.1.1. LCDs

LCDs are a relatively mature technology and are used in display panels, such as smart phone displays, tablet personal computers and televisions. The trends of LCDs are high resolution (7680 × 4320 pixels), ultra-high pixel density of over 300-ppi (pixels per inch) and refresh rate of 240 Hz or higher. To follow these trends, smaller and faster TFTs are required. Consequently, a-IGZO-based TFTs are considered as an advanced method to achieve the high pixel density on a large panel size, due to their high mobility and small size. For example, Baek *et al.* reported a dual-gate synchronized a-IGZO-based TFT for the application of an active-matrix liquid crystal display (AMLCD)[91]. To understand the operation principle of the dual-gate a-IGZO-based TFT under synchronized bias conditions, a mathematical analysis of the dual-gate synchronized a-IGZO-based TFT is analyzed in this work. The equation of current in saturation region is $I_{DS} = W\mu C(V_{GS} - V_{TH})^2/2L$, and the equation of subthreshold swing is $SS = (\partial \log_{10} I_{DS}/\partial V_{GS})^{-1}$, where W and L are the channel width and length, C is the capacitance of the channel semiconductor, and μ is field-effect mobility. Compared with the top-gate, bottom-gate, and synchronized dual-gate a-IGZO TFTs only by bias conditions, from the calculations, the dual-gate a-IGZO-based TFTs under synchronized bias produced larger current and steeper SS compared to the single-gate TFTs with the same channel width/length ratio. These superior properties of the a-IGZO-based TFTs allow the AMLCD to have high pixel density and high resolution. Fig. 10 shows the proposed pixel circuit with the synchronized dual-gate a-IGZO-based TFT for the AMLCD. In the pixel, the switching transistor (a-IGZO-based TFT) was of an inverted staggered structure with an additional gate electrode (top gate). Furthermore, the top gate and the bottom gate were tied together through the sync via, which prevented the dual-gate TFTs from suffering the degradations of the mobility and subthreshold swing. These a-IGZO-based TFTs achieved a smaller size for the same amplitude of drain current.

3.1.2. OLEDs

OLEDs driven by a-IGZO-based TFTs are still in the development stage and they have not been put into the display market on a large scale. For further development, crucial problems such as device stability, imaging uniformity and yield[104–108] need to be solved urgently. For example, the threshold voltage of the a-IGZO-based TFT usually shifts under electrical bias stress[108], which would cause non-uniform brightness in the OLED displays. Fortunately, TFTs with dual-gate structure can control the threshold voltage with little vari-

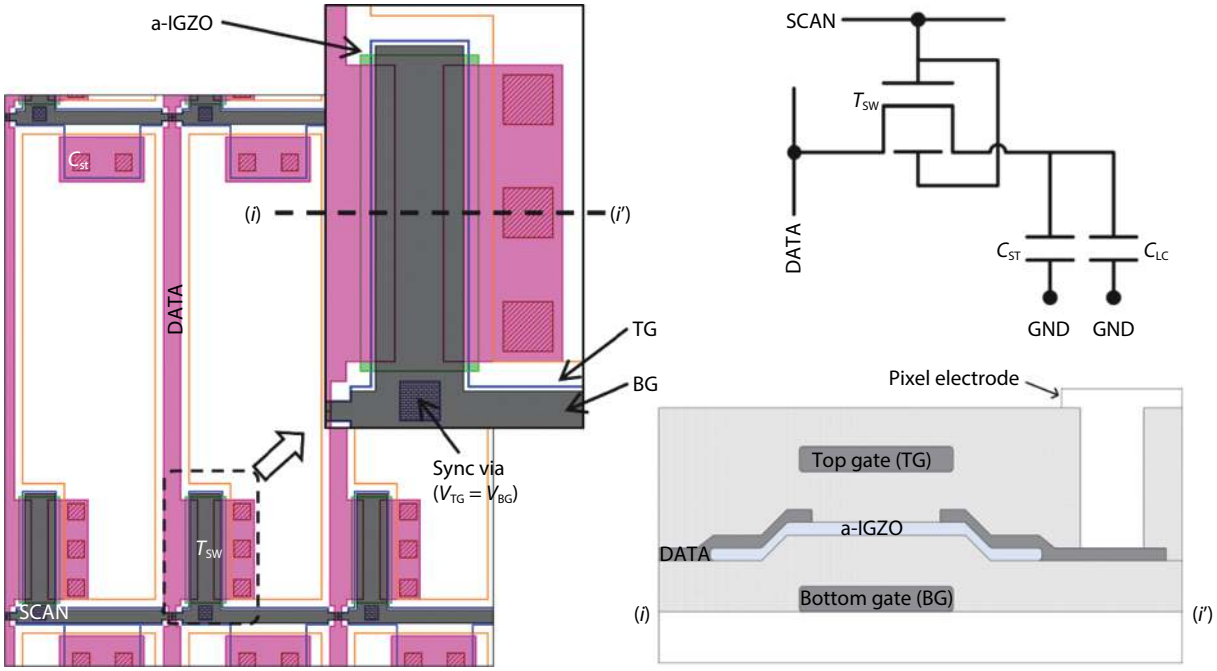

Fig. 10. (Color online) Pixel circuit of the AMLCD based on synchronized dual-gate a-IGZO-based TFTs[91].

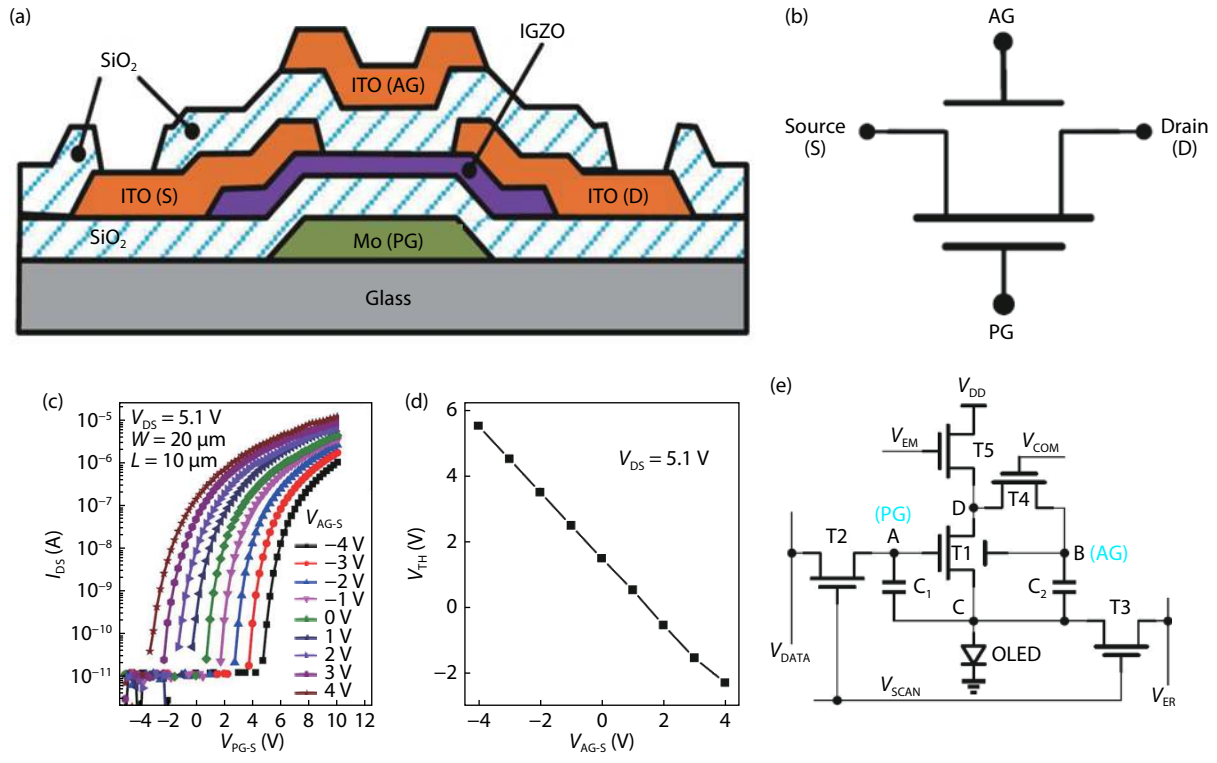

Fig. 11. (Color online) (a) Schematic diagram of the measured dual-gate a-IGZO-based TFT structure. (b) Definition of the electrodes. (c) Transfer curves of the dual-gate a-IGZO-based TFT under primary gate operation with auxiliary gate voltage changing from −4 to 4 V. (d) Threshold voltage as a function of auxiliary gate voltage. (e) Structure of the pixel circuit[101].

ation[101]. Wang *et al.* reported a dual-gate a-IGZO-based TFT-driven pixel circuit for active-matrix OLEDs (AMOLEDs)[101]. Figs. 11(a) and 11(b) show schematic diagram and the electrode definition of the dual-gate TFT structure, respectively. The bottom gate and the top gate were defined as the primary gate and the auxiliary gate, respectively. The threshold voltage of the dual-gate TFT under the primary gate operation can be modulated by the auxiliary gate voltage. Fig. 11(c) shows the transfer curves of the dual-gate a-IGZO-based TFTs under the primary gate operation with auxiliary gate voltage changing from −4 to 4 V. As shown in Fig. 11(d), the threshold voltage shifted linearly with the auxiliary gate voltage. Therefore, the V_{th} variation under the primary gate operation could be compensated by varying auxiliary gate voltage. Fig. 11(e) shows a schematic of the pixel circuit including one driving TFT (T1), four switching

TFTs (T2–T5) and two capacitors (C1 and C2).

3.1.3. Flexible displays

Flexible IGZO-based TFTs are capable for use as flexible displays, due to the unique advantages such as light-weight substrates[87, 109–112], low-voltage-driven[113], and bendability[114, 115]. In addition, when the IGZO thin films are deposited on to suitable substrates, the IGZO-based TFTs can be used to form fully transparent flexible displays. Flexible displays driven by IGZO-based TFTs have been researched in many works[13, 31, 34, 116]. For example, in 2009, Park *et al.* fabricated a 6.5 inch full-color flexible AMOLED on the polyimide (PI) substrate driven by a-IGZO-based TFTs[13]. The a-IGZO-based TFT showed a V_{th} of 0.9 V, an SS of 0.25 V/dec, a μ_{FE} of 15.1 cm^2/(V·s). Moreover, there was no performance degradation under bending of the R = 3 mm. Nag *et al.* presented a top-emitting quarter-quarter-video-graphics-array AMOLED display with 85-ppi resolution driven by a-IGZO-based TFTs[31]. In this display panel, the driven a-IGZO-based TFT showed high electronic characteristics of μ_{FE} of 12.0 cm^2/(V·s), SS of 0.5 V/dec, and I_{on}/I_{off} of over 10^7.

Most TFT gate drivers integrated on the display panel use carry signals between the stages. However, in the flexible display the error of the stressed stages is accumulated through the carry signals when the display panel is bent. This problem will probably lead to the failure of the image refresh. To deal with this problem, Kim *et al.* reported a carry-free gate driver for flexible displays using a-IGZO-based TFTs[117]. This carry-free gate driver overcame that problem because it did not use the carry signals and each unit stage operated independently. Fig. 12(a) shows the conceptual architecture and the output waveforms of the carry-free gate driver. Each unit stage works as a decoder and the output of each stage is decided by the binary-weighted decoder signals. When the mechanical stress is applied, the outputs of the stressed stages would become slower but the errors could not accumulate because there are no carry signals through which the error can propagate and each stage works independently. As shown in Fig. 12(b), the flexible display with a carry-free gate driver can keep the normal operation, even under the mechanical stress. Moreover, the carry-free gate driver showed no voltage fluctuation at the outputs after 10 000 cycles bending test with a bending radius of 2 mm. These carry-free gate drivers achieve high reliability under mechanical stress compared with the traditional carry-type gate drivers for flexible displays.

Table 1 shows the recent studies of the display applications driven by the a-IGZO-based TFTs. This table shows the substrate, structure, electrical properties of the a-IGZO-based TFTs, the size of the display panel and the specific application.

Nowadays, a-IGZO-based TFTs have attracted considerable attention thanks to their large-size, high-resolution and narrow-bezel display applications. Fig. 13 shows this progress in display applications. For example, China Star Optoelectronics Technology (CSOT) developed an 85-inch 8k4k LCD driven by the IGZO-based TFTs. The large-size LCD panel is shown in Fig. 13(a)[121]. Fig. 13(b) shows a 1058-ppi ultra-high-resolution flexible OLED display using IGZO-based TFTs fabricated by Semiconductor Energy Laboratory[62]. Usually, in the display market, displays with a pixel of about 400-ppi

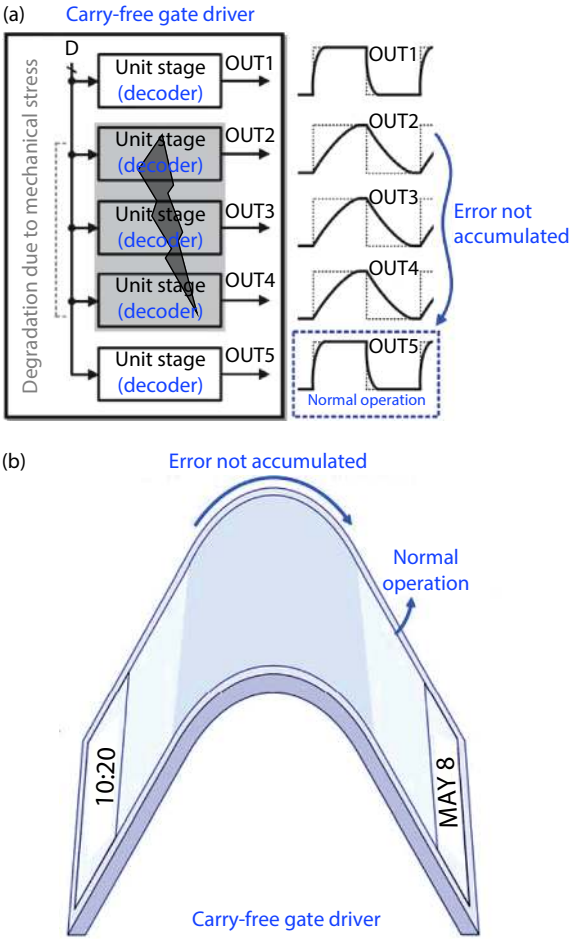

Fig. 12. (Color online) Conceptual architecture and flexible display panel with carry-free gate driver[117].

are used. This OLED display showed an ultra-high resolution of 1058-ppi with *c*-axis-aligned nanocrystalline IGZO materials and could be used for mass production. LG Display demonstrated a bezel free designed AMOLED driven by a-IGZO-based TFTs in 2019[122]. Fig. 13(c) shows an image of the panel. In the fabrication process, this panel is designed to be bezel free. The small remaining bezel of 0.*x* mm is shown in Fig. 13(c), due to the panel cutting process from the mother glass. We believe that in the future displays driven by the IGZO-based TFTs will gradually occupy a dominant position not only in the field of LCD or OELD but also in the field of true flexible displays.

3.2. Sensor applications

Sensors can detect the light, force, voice, gas, humidity *et al.* and transfer them into electrical signal. At present, sensors have been applied in industrial manufacture, healthcare monitoring[123], food safety[124], artificial electronic skins and so on. IGZO-based TFTs are compatible with semiconductor integrated circuit technology and they possess the advantages of small size, room-temperature fabrication process and sensitivity to the pH, pressure, light, gas and so on[16, 20, 22, 23, 25, 125–128], which meet with the requirements of the sensors. In this section, we will present the main sensor applications based on the IGZO-based TFTs.

3.2.1. Photodetectors

Photodetectors have attracted increasing attention, due to their wide applications in biomedicine, fire monitoring,

Table 1. Display applications of the IGZO-based TFTs.

Substrate	Structure of the TFT	μ_{FE} (cm^2/(V·s))	V_{th} (V)	SS (V/dec)	Size (inch)	Application	Ref.
Glass	Dual-gate	11	0.24	130	55	LCD	[118]
Glass	Inverted stagger	9	—	—	32	LCD	[48]
Glass	Bottom gate	15	3.2	0.4	80	LCD	[104]
Glass	Inverted bottom gate	4.2±0.4	−1.3	0.96±0.1	15	AMLCD	[12]
Glass	Back channel etch	7.35	1.6	—	—	AMLED	[100]
Glass	Staggered bottom gate	8.2	1.1	0.58	12.1	AMOLED	[11]
—	—	18.45	1.04	0.73	—	AMOLED	[97]
Glass	Etch stopper	20	—	—	4.8	AMOLED	[103]
Polyimide	Staggered bottom gate	17.3	0.86	0.21	11.7	Flexible AMOLED	[119]
Polyimide	Inverted staggered bottom gate	11.6	1.6	0.25	3	Flexible AMOLED	[34]
Polyimide	Coplanar	10.25	0.34	0.22	—	Flexible OLED	[120]

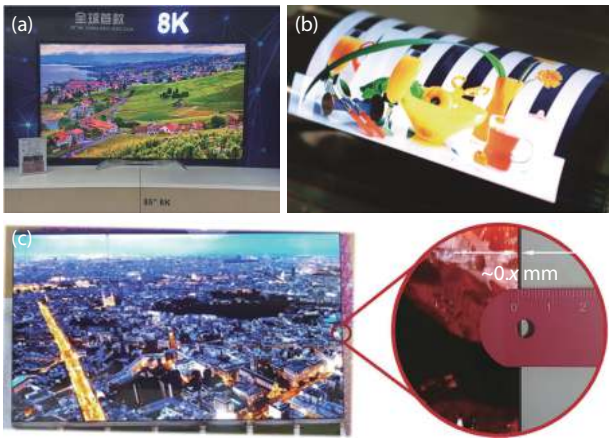

Fig. 13. (Color online) Picture images of the display panels of large size, high-resolution and narrow bezel[62, 121, 122].

photo-communication, missile plume detection and so on. The photodetectors based on the IGZO-based TFTs exhibit a relatively high response to light with a wavelength lower than 420 nm because the IGZO materials possess a wide bandgap over 3.0 eV. For example, Yu *et al.* presented an ultraviolet (UV) photodetector based on the IGZO-based TFT with a p–n junction[27]. Fig. 14 shows a schematic diagram of the IGZO-based TFT structure, the carrier transmission process under the light and the photo responsivity of the IGZO and PEDOT:PSS/SnO_x/IGZO TFTs, respectively. The p–n junction was composed of the PEDOT:PSS/SnO_x/IGZO heterojunction structure. Through the p–n junction, the directional carrier transfer of the photo-generated carriers was experimentally validated. A photo responsivity of 984 A/W at a wavelength of 320 nm was obtained in this work. This work has successfully fabricated a visible-blind ultraviolet photodetector based on the a-IGZO TFTs and achieved ultra-low-power dissipation of lower than 10 nW under illumination and about 0.2 pW in the dark. Moreover, this photodetector with high photoresponsivity has the unique advantage of pixel integration, which can potentially be applied in high performance visible-blind ultraviolet photodetector pixel arrays. Besides the UV photoelectric sensors, the IGZO-based TFTs with narrow-bandgap materials such as graphene dots[129], silver nanoparticles[130] and polymer[131] have successfully been used in visible-light photoelectric sensors. For example, in 2010, Zan *et al.* demonstrated a visible-light phototransistor that consisted of a wide-bandgap a-IGZO and a narrow-bandgap (about 2 V) poly (3-hexylthiophene) (P3HT)[131]. The a-IGZO thin film and P3HT formed a p–n junction diode. The P3HT layer has a high absorption coefficient for visible light and absolutely absorbs visible light, and consequently injects electrons into the a-IGZO layer. As a result, the concentration of the carriers in the channel and also the threshold voltage of the a-IGZO-based TFT change rapidly with the illumination. In this work, the authors proposed a simple way to convert a wide-bandgap a-IGZO-based TFT into a visible-light photodetector that has a fast response and a high sensitivity. Although ultraviolet and visible-light phototransistors have been fabricated in many works, there are few reports of infrared photodetectors based on IGZO TFTs. Lee *et al.* for the first time characterized the infrared photoresponse principle through the subgap density-of-states over the forbidden bandgap of a-IGZO[26]. The origin of the sub-bandgap ($hv < E_g$) photo response in a-IGZO-based TFTs was that the electrons were optically pumped from the photo-responsive sub-bandgap states. From these works, we can see that the photodetectors based on the IGZO-based TFTs have been investigated from ultraviolet to infrared. These works provide useful results that can help the integration of the photodetectors based on the IGZO-based TFTs.

3.2.2. Pressure sensors

Pressure sensors are used to monitor pressure magnitude and fluctuation, which are important in areas such as blood flow, heartbeat, and respiratory system of the human body[132]. Piezoelectric sensors have attracted much attention because they can generate an electric potential in response to an applied pressure. Geng *et al.* proposed a pressure sensor based on a dual-gate a-IGZO-based TFT with a polyvinylidene fluoride (PVDF) piezo-capacitor[133]. When the pressure is applied by finger pressing, the potential of the top-gate will change, thus the threshold voltage of the a-IGZO TFT shifts, which will produce an obvious output signal in the range of 200–300 mV. Fig. 15(a) shows the structure of a dual-gate a-IGZO-based TFT with a piezo-capacitor. The unique advantage of the double gate structure is that the electrical characteristics of the TFT can be simultaneously controlled both by the bottom gate and top gate. In this structure, the piezo-capacitor was formed on the top of a floating top gate. The piezo-capacitor was polarized and generated a voltage to the top gate when it was pressed. Fig. 15(b) shows the transfer curves of the dual-gate a-IGZO-based TFT. From the curves, the V_{th} of the dual-gate a-IGZO-based TFTs shifted to the positive bottom-gate voltage direction by applying negative top-gate voltage, and to the negative bottom-

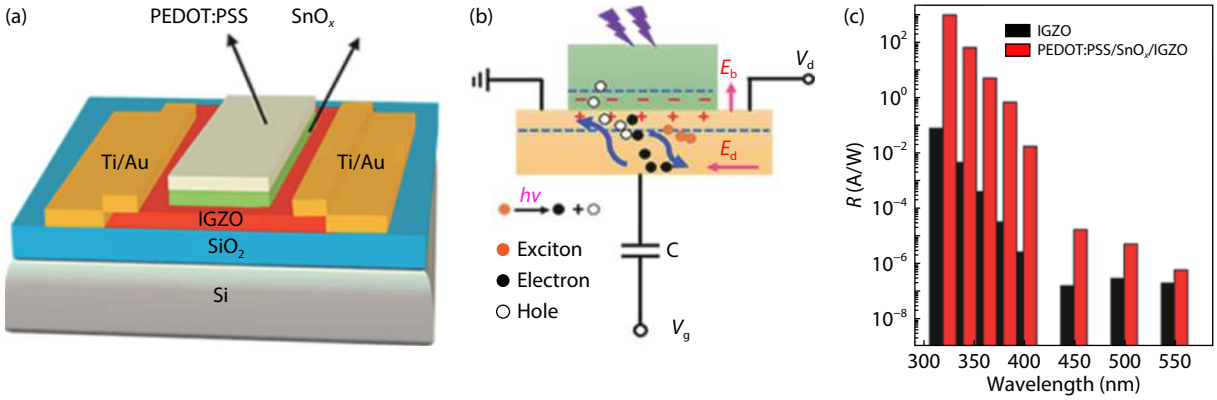

Fig. 14. (Color online) (a) A schematic diagram of the IGZO-based TFT structure. (b) The separation and collection process of the photo-generated carriers. (c) Photoresponse of the IGZO and PEDOT:PSS/SnO_x/IGZO phototransistors as a function of the light wavelength[27].

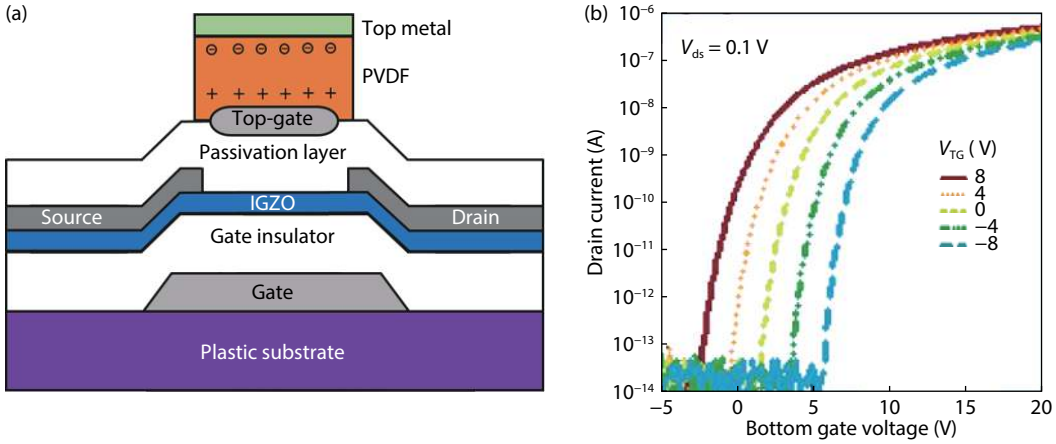

Fig. 15. (Color online) (a) Schematic diagram of the a-IGZO-based TFT pressure sensor structure. (b) Transfer characteristics of the dual-gate TFT with different top-gate voltage[133].

gate voltage direction by applying a positive top-gate voltage. Moreover, the V_{th} would return to its initial value after removing the top-gate voltage. This change of the V_{th} with different top-gate voltage is the mechanism of the pressure sensors. This work has realized a pressure sensor using piezo-capacitor that integrated with dual-gate a-IGZO-based TFTs.

3.2.3. pH sensors

Biosensors have attracted considerable interest for disease diagnosis and the pursuit of a better life. In particular, pH sensors play an important role in clinical medicine, environmental monitoring, agriculture and food engineering[18, 134, 135]. IGZO-based TFTs possess the advantages of compatibility with flexible substrates, chemical/electrical stability and micro/nano size, which are satisfied with the pH sensors[19, 136]. For example, Smith *et al.* presented a flexible extended-gate ion-sensitive field-effect transistor (ISFET) biosensor based on the IGZO-based TFTs using LED technology[19]. The ISFETs are well used as pH sensitive biosensors with different dielectrics such as SnO_2[136], TiO_2[126] and ITO[19] as the pH sensitive layers[18, 125]. In this work, the ISFET drain current was increased as the pH decreased, which was due to the H^+ ion protonation of the ITO extended-gate electrode surface. When the H^+ concentration increased around the surface of the ITO gate electrode, negative charge carriers in the channel were generated thanks to the increased positive charge at the ITO/IGZO interface with decreasing pH value, resulting in the increase of the drain current. Fig. 16(a) shows the structure of a flexible ISFET pH sensor. In this structure, a

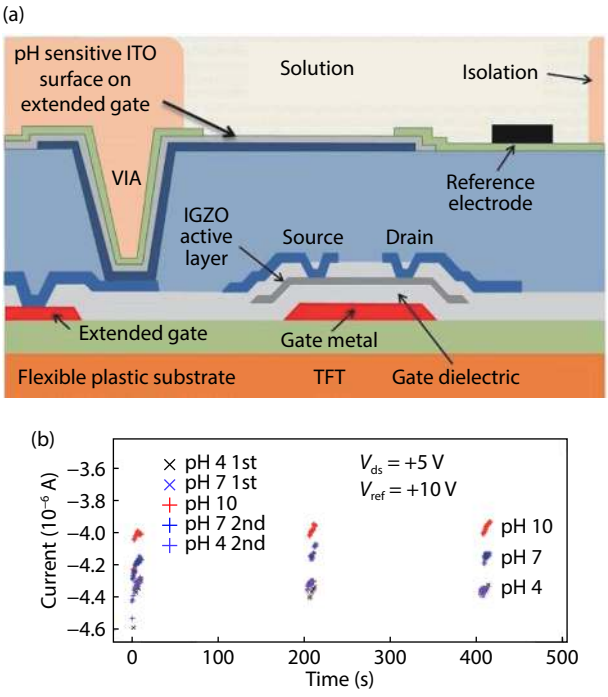

Fig. 16. (Color online) (a) Structure of the flexible extended-gate ISFET pH sensor. (b) Data graph of the drain current vs time[19].

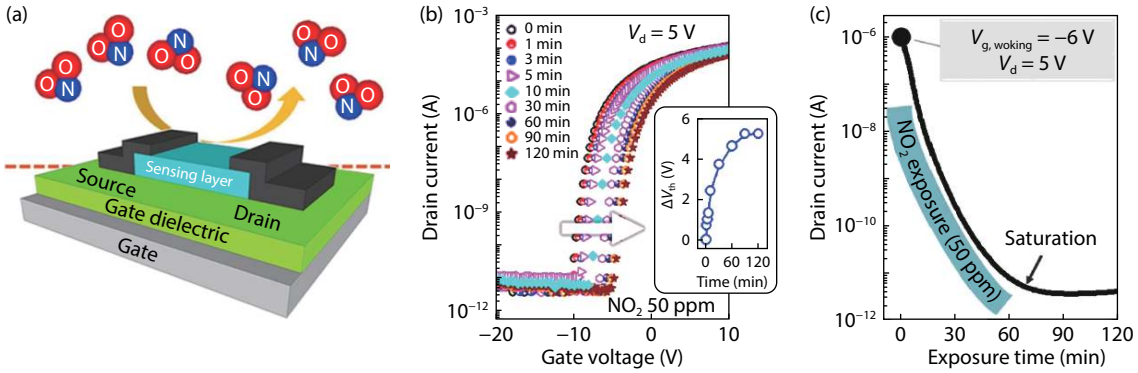

Fig. 17. (Color online) (a) Schematic diagram of the IGZO-based TFT structure. (b) Transfer curves with different time under 50 ppm NO_2 gas concentration. (c) Drain current vs time under 50 ppm NO_2 gas concentration[137].

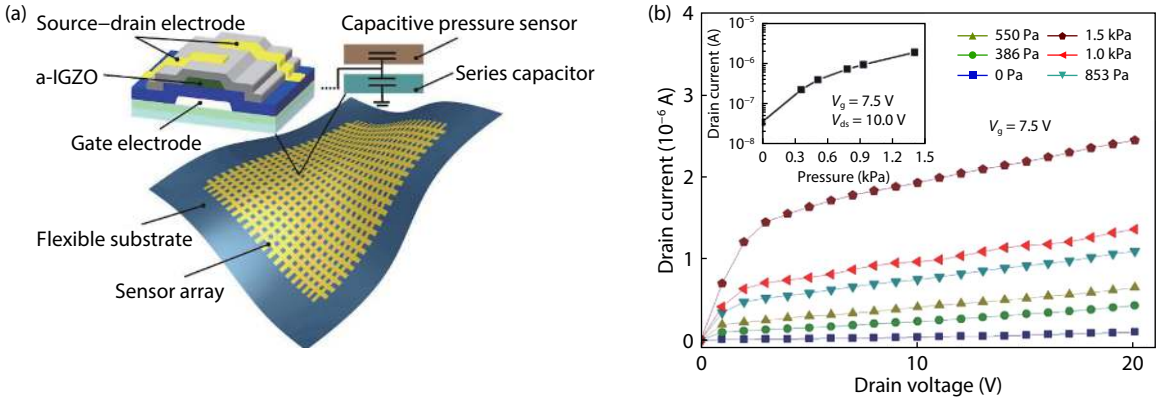

Fig. 18. (Color online) Schematic diagrams of the a-IGZO-based TFT pressure-sensing system and output curves[22].

flexible 125 μm thick polyethylene naphthalate (PEN) plastic was used as the substrate. The top 1 × 3 mm^2 indium tin oxide (ITO) layer was used as the extended gate to detect the pH value. A width/length = 9/9 μm IGZO layer was used as the n-channel. Fig. 16(b) shows the graph of the ISFET drain current vs time. A sequence of pH 4→ pH 7 → pH 10 → pH 7 → pH 4 with the interval of 400 s for each pH concentration was used to test the current. The current was tested from 0 to 10 s, 200 to 210 s, 400 to 410 s. As the pH concentration increased from pH 4 to pH 10, the drain current decreased because of the decrease of the H^+ ion protonation in the ITO extended-gate electrode surface. These results of sensors fabricated on a flexible substrate demonstrate the initial possibility of directly using the flexible LED technology to produce low cost, good performance and flexible IGZO TFT-based biosensors.

3.2.4. Gas sensors

Gas sensors based on IGZO-based TFTs are used to detect both oxidizing and reducing gases (like NO_2 and H_2)[29, 137–139]. Oxidizing or reducing gas molecules act like electron acceptors or donors to change the carrier concentration, respectively, and thus change the drain current of the IGZO-based TFTs[30]. For example, Lee *et al.* reported a H_2 sensor using the IGZO-based TFTs[138]. Palladium (Pd) was used as source/drain electrodes and also used to detect hydrogen (H_2) gas concentration. The drain current increased as the Pd and IGZO interface barrier height decreased, which happened because of the formation of a hydrogen dipole layer at the interface[139]. To sense the reducing gas, Kim *et al.* presented a low-concentration NO_2 gas detector. The a-IGZO thin film was used both as a channel and as a sensing layer[137]. Fig. 17 shows the device structure, transfer curves under 50 ppm NO_2 gas concentration with different times, and the drain current change as a function of the exposure time, respectively. The threshold voltage positive shifted with an oxidation reaction in the NO_2 gas, NO_2 (gas) + e^- (surface of oxide) → NO_2 (adsorbed). In particular, the sensing data was accurately obtained from the variation of the drain current and this sensor achieved efficient detection of the variation of the NO_2 concentration. Thus, a-IGZO TFT-based gas sensors show good responsivity, sensitivity and recovery from the low concentration of the NO_2 gas.

3.2.5. Flexible sensors

IGZO-based TFT sensors have been widely used in flexible light detectors, pH sensors, gas detectors, and so on[19, 22, 33, 140]. For example, Xin *et al.* presented a novel pressure-sensing system using an a-IGZO-based TFT configuration comprised of a microstructured polydimethylsiloxane (PDMS) capacitor[22]. Fig. 18 shows the structures and the output curves, respectively. This array was fabricated on a highly flexible PI substrate using the back channel etch structure. The mechanism of the device can be explained by the change of the capacitance of the microstructured PDMS under an external pressure to modulate the gate voltage and change the output drain current. This device shows sufficient sensitivity to detect pressure difference under extremely low-pressure regime. The microstructure PDMS thin film showed good sensitivity of 0.1 kPa^{-1} and response time

Table 2. Sensor applications of the IGZO-based TFTs.

Substrate	Structure of the TFT	μ_{FE} ($cm^2V^{-1}s^{-1}$)	I_{on}/I_{off}	V_{th} (V)	SS (V/dec)	Application	Ref.
SiO_2/Si	Top gate	18	~10^6	0.6	0.07	Photoelectric sensor	[145]
Si	Bottom gate	10.8	—	2.3	0.34	Phototransistor	[131]
Glass	Bottom-gate	3	1.08×10^5	0.5	0.49	Deep-ultraviolet phototransistor	[146]
SiO_2/Si	Double gate	6.51	5×10^6	0.51	0.12	PH sensor	[136]
Si	Double gate	4	10^7	2.8	0.31	PH sensor	[126]
SiO_2/Si	Bottom gate	7.58	~10^7	—	0.49	Gas sensor	[147]
—	Double gate	13.8	2.9×10^6	0.72	0.19	Hybrid gas sensor	[30]
Glass	Bottom gate	12	—	1.39–1.92	0.24	Temperature sensor	[16]
Metal foil	Bottom gate	21	~10^7	7.36	1.12	Flexible thermal and pressure sensor	[148]
Polyimide	Back channel etch	20	10^7	1	—	Flexible pressure sensor	[149]
Polyethylene naphthalate	Bottom-gate	—	—	—	—	Biosensor	[19]
Polyethylenenaphthalate	Bottom-gate staggered	10~15	—	2	0.3	Flexible X-Ray detector	[150]
Polyimide	Bottom-gate inverted staggered	13.34	—	0.87	—	Flexible gas sensor	[140]

of lower than 190 ms for the pressure of 12 kPa. According to the amplification effect of the a-IGZO-based TFT, the device showed a high sensitivity in the subthreshold region for the ultra-low-pressure (⩽ 1.5 kPa) detection and good linearity in the linear region for low-pressure (⩽ 7 kPa) detection. The results demonstrated that a novel approach can be used for pressure-sensing intelligent products.

Flexible IGZO-based TFTs are especially capable for use as flexible circuits, such as oscillators, inverters, radio frequency identifications, operational amplifiers and clock generators[87, 141–143]. Thus, flexible sensors provided by flexible circuits have aroused a great deal of interest[47, 144]. For example, Meister *et al.* reported a low-power low-frequency light-sensing oscillator with IGZO-based TFTs that were integrated on a bendable plastic substrate[47]. This oscillator could be directly used as a light sensor without additional read out circuits. The device oscillated between 5 Hz in the dark and 31 Hz under daylight. The light-sensitivity of the oscillation frequency is between 7.4 Hz/klx in the dark and about 1.7 Hz/klx in the daylight. In particular, this device had a low frequency of 5–31 Hz and low power of 188 μW. Significantly, this work achieved a low-power consumption, flexible integrated circuit that can be directly used to sense the light intensity through the frequency of the oscillation in a small chip area.

Table 2 shows the recent studies of the sensor applications based on the IGZO-based TFTs. This table shows the substrate, structure, electrical properties and the specific sensor applications of the IGZO-based TFTs.

3.3. Neuromorphic systems

Traditional computers based on von Neumann architectures play essential roles in almost every field and have led to the development of information technology. However, there are two main problems that hinder the further improvement of computing power: the first is the limitation on energy efficiency as we approach the end of the Moore's law and the second is the challenge of the von Neumann bottleneck. According to Moore's law, device size was made smaller and smaller. However, at present, the device size is close to the physical limit and Moore's law is gradually failing. Meanwhile, information processing in the von Neumann computer requires the transmission between processor and memory units, which is unfavorable for computational efficiency and the size of the architecture. As computing speed increases, the energy consumption becomes larger. In the famous man-machine battle, the power of the artificial intelligence AlphaGo is about 150 kW. These problems of von Neumann computers will become more serious with the spread of the Internet of Things and artificial intelligence. As an efficient solution for complex data processing, neuromorphic electronics that emulate the functions and the information processing of the human brain have been proposed.

The human brain is a highly efficient computing system that can process input information and react to external stimuli with ultralow energy consumption of ~20 W and small volume occupation of ~1200 cm^3 [151]. Neurons are often considered as the computational engines of the human brain. The signals conducted between neurons depend on the recent activities at either or both sides of the synapse. The connection strength between synapses is known as synaptic plasticity. Synaptic plasticity consists of three different styles: 1) long-term plasticity, in which the change of synapses can last for hours or longer and is considered to be memory; 2) homeostatic plasticity, which keeps the neurons in an appropriate state; and 3) short-term plasticity, in which the signals that occur in the synapses last for milliseconds or minutes, and is considered as a critical computational function in neural systems. Synapses are the basic units of computing and learning in the human brain. To build artificial neuromorphic systems inspired by the human brain, the basic requirement is to prepare a device that can simulate synaptic behaviors. In the past few years, complementary metal oxide semiconductor (CMOS) integrated circuits have been used to mimic the synaptic functions, such as IBM's TrueNorth chip that integrated 5.4 billion transistors to simulate 1 million neurons and 256 million synapses[152]. However, large-scale CMOS-based analog circuits consume a large amount of energy, which hinders the development of the CMOS synaptic applications. In recent years, the design of a single device that mimics syn-

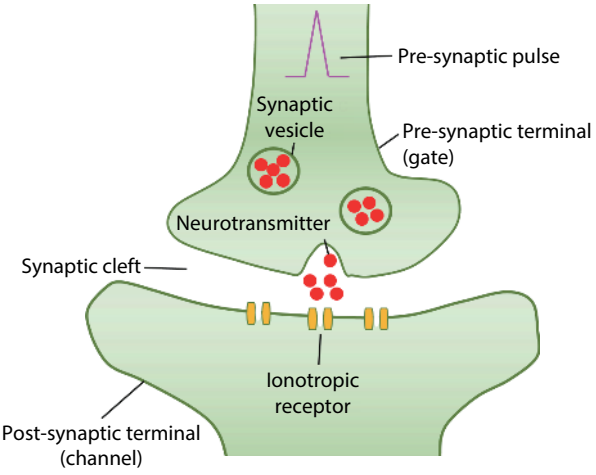

Fig. 19. (Color online) Schematic diagram of an artificial synapse based on neuromorphic transistor.

aptic functions has received a lot of attention, such as two-terminal memristors[153–156]. Two-terminal memristors consist of three layers, two electrodes for sending and receiving information, and a 'storage' layer between them to memorize the information. Although two-terminal memristors possess the advantages of small size, simple device structure and low-energy consumption, the instability of the device and the integration difficulty may hinder their application in neuromorphic systems. Recently, three-/multi-terminal transistors have attracted much attention[157]. Unlike two-terminal memristors, these transistors have a gate to control the channel conductance and the energy consumption of the device can be lower. Furthermore, three-/multi-terminal transistors have good stability, controllable parameters and easy integration. For the emulation of synaptic behaviors, as shown in Fig. 19, the gate electrode is used as the presynaptic terminal and the channel layer with source/drain electrodes is considered as the postsynaptic terminal. The information transmission and process in the synapse starts from the triggering of the presynaptic pulse. Then, electrical activities in the pre-synapse are converted to the release of neurotransmitters and the post-synapse receives the neurotransmitters. Consequently, the current/potential of the post-synapse is changed. When a pulse voltage is applied to the gate electrode, the conductance of the channel layer is changed, which can be measured by applying a small voltage between the source and drain electrodes.

Herein, we will demonstrate the works reported by our group about the application of IGZO-based TFT in synaptic networks and neuromorphic systems[35–37, 42, 43, 45, 158–161]. As early as 2009, Jiang and Wan *et al.* reported the first ultralow-voltage IGZO-based electric-double-layer (EDL) TFT[44]. This TFT exhibited an ultralow operation voltage about 1.0 V, a high μ_{FE} of 28.5 $cm^2/(V{\cdot}s)$, and a low SS of 110 mV/decade. This ultralow-voltage operation was ascribed to the large EDL capacitance. Usually, in a liquid or solid electrolyte, mobile cations and anions are filled between two electrodes. When an external voltage is applied to the electrodes, the cations and anions will move to the surface of electrolyte/electrode, respectively, which is the charging process and will contribute a large EDL capacitance[162]. In our work, the proton H^+ in mesoporous SiO_2 moved from one bridging oxygen atom to another. When a negative dc voltage was applied to the gate electrode, the H^+ would move to the dielectric/channel interface. Simultaneously, the electrons in the n-type IGZO channel accumulated near the interface, due to the combination of the gate potential bias. Importantly, this work laid a solid foundation for the follow-up research of IGZO-based TFT artificial synapse devices.

It is essential for synaptic transistors to have low-energy consumption. Zhou and Wan *et al.* presented flexible EDL IGZO-based TFTs with the energy consumption as low as 0.23 pJ/spike[161]. In this work, short-term synaptic plasticity and high-pass filtering behaviors are also mimicked. Figs. 20(a) and 20(b) show the structure of the device and a simple image of the artificial synapse, respectively. The artificial synapse is composed of an IGZO transistor. The gate is considered as the pre-synapse and the channel is considered as the post-synapse. When the voltage pulse is applied to the gate, a spike could be measured in the drain electrode, which simulates the information transfer process in the synapse. Fig. 20(c) shows the paired-pulse facilitation (PPF) curve that the excitatory postsynaptic current (EPSC) triggered by a pair of gate voltage spikes. The PPF reached a maximum value of 192% when the time interval was 20 ms, and it was reduced to 100% because the time interval is long enough. When the time interval between the pair of gate voltage spikes is shorter than the relaxation time of the protons in the nanogranular P-doped SiO_2, some of the protons could not diffuse back to their equilibrium position before the second spike arrives, causing a large PPF. However, with the increase of the interval time, the protons gradually move back to their equilibrium position and the PPF gradually decreases. Fig. 20(d) shows the EPSC amplitude gain as a function of spike frequency. As the frequency of the voltage train changed from 1 to 50 Hz, the gain increased from ~1.0 to ~3.7. These results demonstrate the high-pass synaptic dynamic filtering of the IGZO-based neuromorphic TFTs.

Emulation of the short-term synaptic plasticity and synaptic filtering based on IGZO-based EDL TFTs was proposed by Wan *et al.*[45]. To simulate the synaptic facilitation and depression function, a three-terminal device was reduced to a two-terminal synaptic device. High-pass and low-pass filtering were successfully simulated. Figs. 21(a) and 21(b) show schematic images of the IGZO-based EDL TFT. In Fig. 21(a), the drain electrode and gate electrode were shortly connected as the presynaptic terminal. When we applied a positive voltage to the drain electrode, the protons in the electrolyte migrated to the IGZO channel/electrolyte interface. The EPSC was increased and the facilitation simulation was achieved. Fig. 21(b) shows that the source electrode and gate electrode were shortly connected as post-synapse terminal to emulate the short-term depression behavior. When the positive spike was applied to the drain electrode, the protons in the electrolyte migrated to gate electrode/electrolyte interface. The response current gradually reduced and synaptic depression can be obtained. Figs. 21(c) and 21(d) show the facilitation and depression simulations with the EPSC as a function of the pulse number and rate, respectively.

Our brain contains more synapses than neurons, which guarantees multiple information processing. It is suggested that the multi-terminal neuro transistors are more suitable for complex neural network simulation[163]. He and Wan *et al.* proposed capacitively coupled multi-terminal IGZO-based neur-

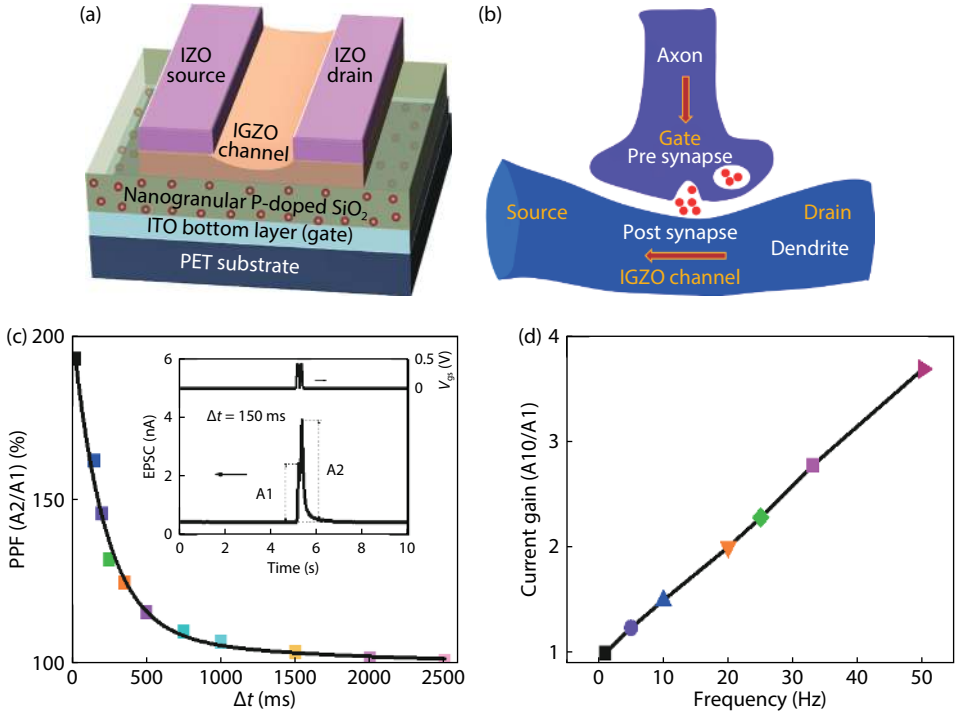

Fig. 20. (Color online) (a) Schematic diagram of the electric-double-layer (EDL) IGZO-based neuromorphic TFT structure. (b) Simple schematic diagram of an artificial synapse based on the IGZO-based TFT. (c) PPF ratio as a function of the time interval between the two stimuli spike. (d) EPSC amplitude gain as a function of spike frequency[161].

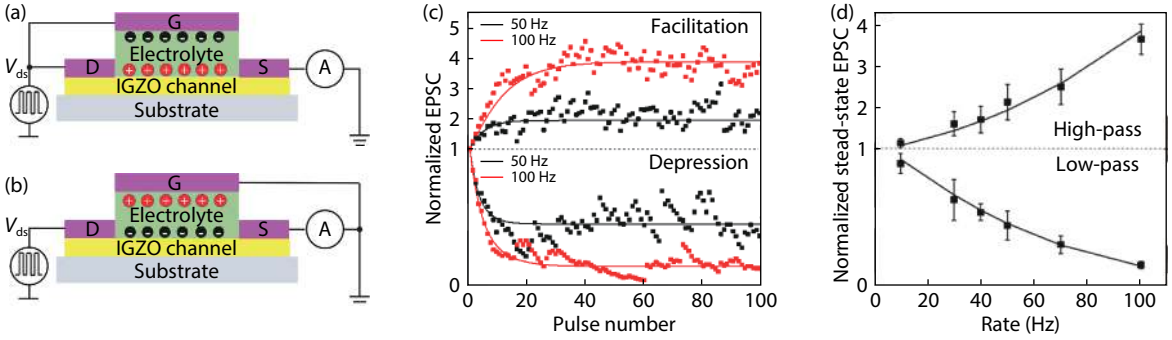

Fig. 21. (Color online) (a, b) Schematic images of the top-gate IGZO-based neuromorphic TFTs with electrolyte gate dielectric. (c, d) EPSC as a function of pulse number and rate of the positive presynaptic spike trains, respectively[45].

omorphic TFT and neural network for spatiotemporal information processing[36]. The multi-gate terminals and the channel of the TFT are coupled by strong lateral ionic/electronic coupling effect. In the simulation, electric pulse sequences applied on the multi-gate are used as spatiotemporal information and the response is read from the source/drain. Multi-gate terminals and source/drain electrodes are used as presynaptic neuron (PREN) terminals and postsynaptic neuron (POSTN), respectively. A neural network consisting of two PRENs and POSTNs was proposed to emulate the sound azimuth detection as shown in Fig. 22(b). PREN1 and PREN2 are used as left and right ear sensing neurons, respectively. Fig. 22(a) shows a schematic diagram of sound location of the ears. An electrical pulse is applied on PREN2 and then the same pulse is applied on PREN1 when the sound is from the right direction, and vice versa. The time interval represents the sound azimuth. Fig. 22(c) shows that the POSTN1 and POSTN2 could produce different response (I_{POST1} and I_{POST2}) to the sound direction. Fig. 22(d) shows that the ratio of the amplitude of I_{POST2} and I_{POST1} varies with the sound azimuth. Thus, the neural network can realize sound azimuth detection function. A network that can realize spatiotemporal information processing is of great interest for brain-like computing in the future.

4. Conclusions and outlook

In this review, we have discussed IGZO materials, devices and recent developments of the IGZO-based TFT applications. In the introduction, the history, electron travelling orbitals and deposition methods of the IGZO materials are presented. Then, capitalizing on the unique properties of IGZO-based TFTs, such as relatively high mobility, good optical transparency and good compatibility with traditional CMOS technology, numerous devices based on IGZO-based TFTs have been demonstrated. For these applications, IGZO-based TFTs are not only promising candidates for display applications

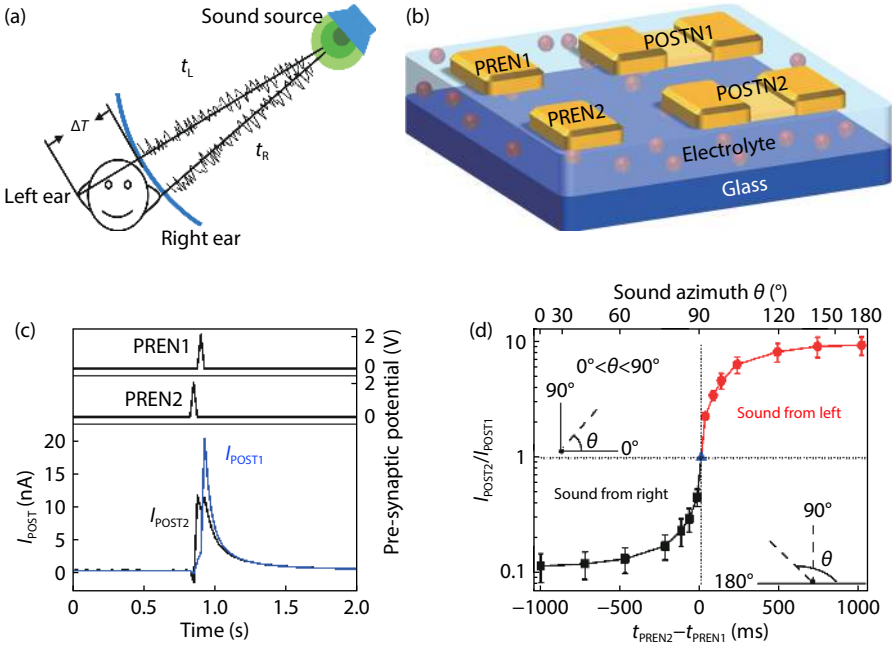

Fig. 22. (Color online) (a) Schematic diagram of sound location of the human brain. (b) Schematic picture of the IGZO neuromorphic device and neural network for the emulation of sound azimuth detection. (c) I_{POSTN1} and I_{POSTN2} when the sound comes from the right direction. (d) The ratio of I_{POST2} and I_{POST1} as a function of the sound azimuth[36].

but are also actively involved in sensor applications and neuromorphic systems.

Great progress has been made in implementing IGZO-based TFTs into mainstream display technologies such as LCDs and OLEDs. However, the brightness uniformity of the panel, the stability of the device and the yield hinder the progress of the high ppi, the large size, the narrow bezel and the true flexible display panels. We believe that these problems will be overcome in the not-too-distant future and that the IGZO-based TFTs will gradually dominate the display market. The application of display derivers may be the main development direction of the IGZO-based TFTs in the future.

Based on the state-of-the-art understanding of the properties of the IGZO-based TFTs, multifunctional sensors such as photoelectric sensors, pressure sensors, pH sensors and gas sensors have been fabricated. Nevertheless, the low detection precision hinders their further application in the field of sensing. For pH sensors, the pH sensitivity based on the ISFET is limited by the Nernst limit of about 59 mV/pH. For photoelectric sensors, the persistent photoconductivity effect has greatly limited the detection accuracy. However, by optimizing thin-film fabrication strategies, the structure of the device and the fabrication technology, it is predicted that sensors based on IGZO-based TFTs will appear in consumer products.

Although some neuromorphic devices based on IGZO-based TFTs have been fabricated and some important synaptic/neuronal functions have been emulated, the development of the emerging neuromorphic device and system is still in its early stage. There is still a lot of room for optimization in device technology and structure. In the future, three-dimensional integration is one of the most important issues for a large-scale neuromorphic system. Finally, the key challenge for brain-like computing and perception is to explore and understand the spatiotemporal dynamic algorithm used in our brain. Consequently, interdisciplinarity between microelectronics and neuroscience is crucial for disruptive innovation in neuromorphic system.

Acknowledgements

The authors are grateful for the financial support from the National Natural Science Foundation of China (Grant No. 62074075, 61834001), and the National Key R&D Program of China (Grant No. 2019YFB2205400).

References

[1] Kimizuka N, Mohri T. Spinel, $YbFe_2O_4$, and $Yb_2Fe_3O_7$ types of structures for compounds in the In_2O_3 and Sc_2O_3–A_2O_3–BO systems [A: Fe, Ga, or Al; B: Mg, Mn, Fe, Ni, Cu, or Zn] at temperatures over 1000 °C. J Solid State Chem, 1985, 60, 382

[2] Nomura K. Thin-film transistor fabricated in single-crystalline transparent oxide semiconductor. Science, 2003, 300, 1269

[3] Nomura K, Ohta H, Takagi A, et al. Room-temperature fabrication of transparent flexible thin-film transistors using amorphous oxide semiconductors. Nature, 2004, 432, 488

[4] Arai T. Oxide-TFT technologies for next-generation AMOLED displays. J Soc Inf Disp, 2012, 20, 156

[5] Lin C L, Lai P C, Lai P C, et al. Pixel circuit with parallel driving scheme for compensating luminance variation based on a-IGZO TFT for AMOLED displays. J Display Technol, 2016, 12, 1681

[6] Kamiya T, Nomura K, Hosono H. Electronic structures above mobility edges in crystalline and amorphous In-Ga-Zn-O: Percolation conduction examined by analytical model. J Disp Technol, 2009, 5, 462

[7] Wellenius P, Suresh A, Luo H, et al. An amorphous indium-gallium-zinc-oxide active matrix electroluminescent pixel. J Disp Technol, 2009, 5, 438

[8] Ito M, Kon M, Ishizaki M, et al. A flexible active-matrix TFT array with amorphous oxide semiconductors for electronic paper. IDW/AD'05, 2005, 845

[9] Lee H N, Kyung J, Kang S K, et al. 3.5 inch QCIF+ AM-OLED panel

based on oxide TFT backplane. SID Symp Dig Tech Pap, 2007, 38, 1826

[10] Ito M, Kon M, Miyazaki C, et al. Amorphous oxide TFT and their applications in electrophoretic displays. Phys Status Solidi A, 2008, 205, 1885

[11] Jeong J K, Jeong J H, Choi J H, et al. 12.1-inch WXGA AMOLED display driven by indium-gallium-zinc oxide TFTs array. SID Symp Dig Tech Pap, 2008, 39, 1

[12] Lee J H, Kim D H, Yang D J, et al. World's largest (15-inch) XGA AM-LCD panel using IGZO oxide TFT. SID Symp Dig Tech Pap, 2008, 39, 625

[13] Park J S, Kim T W, Stryakhilev D, et al. Flexible full color organic light-emitting diode display on polyimide plastic substrate driven by amorphous indium gallium zinc oxide thin-film transistors. Appl Phys Lett, 2009, 95, 013503

[14] Huang J J, Su C Y, Qiao X P, et al. Fabrication of 5.5-inch AMOLED panel using IGZO TFTs. SID Symp Dig Tech Pap, 2019, 50, 157

[15] Choi S, Kim S, Jang J, et al. Oxygen content and bias influence on amorphous InGaZnO TFT-based temperature sensor performance. IEEE Electron Device Lett, 2019, 40, 1666

[16] Jeong H, Kong C S, Chang S W, et al. Temperature sensor made of amorphous indium–gallium–zinc oxide TFTs. IEEE Electron Device Lett, 2013, 34, 1569

[17] Kumar N, Kumar J, Panda S. Low temperature annealed amorphous indium gallium zinc oxide (a-IGZO) as a pH sensitive layer for applications in field effect based sensors. AIP Adv, 2015, 5, 067123

[18] Kumar N, Kumar J, Panda S. Back-channel electrolyte-gated a-IGZO dual-gate thin-film transistor for enhancement of pH sensitivity over Nernst limit. IEEE Electron Device Lett, 2016, 37, 500

[19] Smith J T, Shah S S, Goryll M, et al. Flexible ISFET biosensor using IGZO metal oxide TFTs and an ITO sensing layer. IEEE Sens J, 2014, 14, 937

[20] Geng D, Chen Y F, Mativenga M, et al. Touch sensor array with integrated drivers and comparator using a-IGZO TFTs. IEEE Electron Device Lett, 2017, 38, 391

[21] Tai Y H, Chiu H L, Chou L S. Active matrix touch sensor detecting time-constant change implemented by dual-gate IGZO TFTs. Solid-State Electron, 2012, 72, 67

[22] Chen X, Chen L L, Li T K, et al. Corrections to "highly sensitive flexible pressure sensor by the integration of microstructured PDMS film with a-IGZO TFTs". IEEE Electron Device Lett, 2018, 39, 1262

[23] Smith J T, Couture A J, Stowell J R, et al. Optically seamless flexible electronic tiles for ultra large-area digital X-ray imaging. IEEE Trans Compon, Packag Manufact Technol, 2014, 4, 1109

[24] Xiao P, Huang J H, Dong T, et al. X-ray photoelectron spectroscopy analysis of the effect of photoresist passivation on InGaZnO thin-film transistors. Appl Surf Sci, 2019, 471, 403

[25] Zhao C, Kanicki J. Amorphous In-Ga-Zn-O thin-film transistor active pixel sensor X-ray imager for digital breast tomosynthesis. Med Phys, 2014, 41, 091902

[26] Lee H, Kim J, Kim J, et al. Investigation of infrared photo-detection through subgap density-of-states in a-InGaZnO thin-film transistors. IEEE Electron Device Lett, 2017, 38, 584

[27] Yu J, Javaid K, Liang L, et al. High-performance visible-blind ultraviolet photodetector based on IGZO TFT coupled with p-n heterojunction. ACS Appl Mater Interfaces, 2018, 10, 8102

[28] Tang H Y, Li Y T, Sokolovskij R, et al. Ultra-high sensitive NO_2 gas sensor based on tunable polarity transport in CVD-WS_2/IGZO p-n heterojunction. ACS Appl Mater Interfaces, 2019, 11, 40850

[29] Yang D J, Whitfield G C, Cho N G, et al. Amorphous $InGaZnO_4$ films: Gas sensor response and stability. Sens Actuators B, 2012, 171/172, 1166

[30] Zan H W, Li C H, Yeh C C, et al. Room-temperature-operated sensitive hybrid gas sensor based on amorphous indium gallium zinc oxide thin-film transistors. Appl Phys Lett, 2011, 98, 253503

[31] Nag M, Bhoolokam A, Smout S, et al. Circuits and AMOLED display with self-aligned a-IGZO TFTs on polyimide foil. J Soc Inf Disp, 2014, 22, 509

[32] Han G Q, Cao S G, Yang Q, et al. High-performance all-solution-processed flexible photodetector arrays based on ultrashort channel amorphous oxide semiconductor transistors. ACS Appl Mater Interfaces, 2018, 10, 40631

[33] Honda W, Harada S, Ishida S, et al. High-performance, mechanically flexible, and vertically integrated 3D carbon nanotube and InGaZnO complementary circuits with a temperature sensor. Adv Mater, 2015, 27, 4674

[34] Miura K, Ueda T, Nakano S, et al. Low-temperature-processed IGZO TFTs for flexible AMOLED with integrated gate driver circuits. SID Symp Dig Tech Pap, 2011, 42, 21

[35] Wan C J, Liu Y H, Zhu L Q, et al. Short-term synaptic plasticity regulation in solution-gated indium-gallium-zinc-oxide electric-double-layer transistors. ACS Appl Mater Interfaces, 2016, 8, 9762

[36] He Y L, Nie S, Liu R, et al. Spatiotemporal information processing emulated by multiterminal neuro-transistor networks. Adv Mater, 2019, 31, 1900903

[37] Liu Y H, Zhu L Q, Feng P, et al. Freestanding artificial synapses based on laterally proton-coupled transistors on chitosan membranes. Adv Mater, 2015, 27, 5599

[38] Caughey D M, Thomas R E. Carrier mobilities in silicon empirically related to doping and field. Proc IEEE, 1967, 55, 2192

[39] Moore A R. Electron and hole drift mobility in amorphous silicon. Appl Phys Lett, 1977, 31, 762

[40] Lee J M, Cho I T, Lee J H, et al. Bias-stress-induced stretched-exponential time dependence of threshold voltage shift in InGaZnO thin film transistors. Appl Phys Lett, 2008, 93, 093504

[41] Liao C W. Mobility impact on compensation performance of AMOLED pixel circuit using IGZO TFTs. J Semicond, 2019, 40, 022403

[42] He Y L, Liu R, Jiang S S, et al. IGZO-based floating-gate synaptic transistors for neuromorphic computing. J Phys D, 2020, 53, 215106

[43] He Y L, Nie S, Liu R, et al. Dual-functional long-term plasticity emulated in IGZO-based photoelectric neuromorphic transistors. IEEE Electron Device Lett, 2019, 40, 818

[44] Jiang J, Wan Q, Sun J, et al. Ultralow-voltage transparent electric-double-layer thin-film transistors processed at room-temperature. Appl Phys Lett, 2009, 95, 152114

[45] Wan X, Yang Y, Feng P, et al. Short-term plasticity and synaptic filtering emulated in electrolyte-gated IGZO transistors. IEEE Electron Device Lett, 2016, 37, 299

[46] Pierre A, Doris S E, Lujan R, et al. Monolithic integration of ion-selective organic electrochemical transistors with thin film transistors on flexible substrates. Adv Mater Technol, 2019, 4, 1800577

[47] Meister T, Ishida K, Knobelspies S, et al. 5–31-Hz 188-μW light-sensing oscillator with two active inductors fully integrated on plastic. IEEE J Solid-State Circuits, 2019, 54, 2195

[48] Ma Q G, Wang H H, Zhou L F, et al. Robust gate driver on array based on amorphous IGZO thin-film transistor for large size high-resolution liquid crystal displays. IEEE J Electron Devices Soc, 2019, 7, 717

[49] Wu J, Shi J F, Dong C Y, et al. Effect of active layer deposition temperature on the performance of sputtered amorphous In–Ga–Zn–O thin film transistors. J Semicond, 2014, 35, 014003

[50] Kim Y M, Kang H B, Kim G H, et al. Improvement in device performance of vertical thin-film transistors using atomic layer deposited IGZO channel and polyimide spacer. IEEE Electron Device Lett, 2017, 38, 1387

[51] Sheng J Z, Lee J H, Choi W H, et al. Atomic layer deposition for ox-

ide semiconductor thin film transistors: Advances in research and development. J Vac Sci Technol A, 2018, 36, 060801
[52] Katsouras I, Frijters C, Poodt P, et al. Large-area spatial atomic layer deposition of amorphous oxide semiconductors at atmospheric pressure. J Soc Inf Disp, 2019, 27, 304
[53] Wu C H, Chang K M, Chen Y M, et al. Investigation of electrical characteristics on AP-PECVD fabricated amorphous IGZO TFTs with hydrogen plasma treatment. J Nanosci Nanotechnol, 2019, 19, 2306
[54] Takenaka K, Endo M, Hirayama H, et al. Low-temperature formation of high-mobility a-InGaZnO_x films using plasma-enhanced reactive processes. Jpn J Appl Phys, 2019, 58, 090605
[55] Wu C H, Chang K M, Chen Y M, et al. Study of *in situ* hydrogen plasma treatment on InGaZnO with atmospheric pressure-plasma enhanced chemical vapor deposition. J Nanosci Nanotechnol, 2019, 19, 2310
[56] Kim D J, Kim D L, Rim Y S, et al. Improved electrical performance of an oxide thin-film transistor having multistacked active layers using a solution process. ACS Appl Mater Interfaces, 2012, 4, 4001
[57] Lilienfeld J E. Method and apparatus for controlling electric currents. USA Patent, US1745175, 1930
[58] Weimer P. The TFT a new thin-film transistor. Proc IRE, 1962, 50, 1462
[59] Carcia P F, McLean R S, Reilly M H, et al. Transparent ZnO thin-film transistor fabricated by rf magnetron sputtering. Appl Phys Lett, 2003, 82, 1117
[60] Hoffman R L, Norris B J, Wager J F. ZnO-based transparent thin-film transistors. Appl Phys Lett, 2003, 82, 733
[61] Masuda S, Kitamura K, Okumura Y, et al. Transparent thin film transistors using ZnO as an active channel layer and their electrical properties. J Appl Phys, 2003, 93, 1624
[62] Nagata T, Hirasa S, Dozen Y, et al. A 2.78-in 1058-ppi ultra-high-resolution flexible OLED display using CAAC-IGZO FETs. SID Symp Dig Tech Pap, 2016, 47, 1052
[63] Troughton J, Atkinson D. Amorphous InGaZnO and metal oxide semiconductor devices: An overview and current status. J Mater Chem C, 2019, 7, 12388
[64] Mativenga M, Um J K, Kang D H, et al. Edge effects in bottom-gate inverted staggered thin-film transistors. IEEE Trans Electron Devices, 2012, 59, 2501
[65] Chang K J, Chen W T, Chang W C, et al. A-IGZO TFTs reliability improvement by dual gate structure. SID Symp Dig Tech Pap, 2015, 46, 1203
[66] Li X L, Geng D, Mativenga M, et al. High-speed dual-gate a-IGZO TFT-based circuits with top-gate offset structure. IEEE Electron Device Lett, 2014, 35, 461
[67] Lim H, Yin H X, Park J S, et al. Double gate GaInZnO thin film transistors. Appl Phys Lett, 2008, 93, 063505
[68] Munzenrieder N, Voser P, Petti L, et al. Flexible self-aligned double-gate IGZO TFT. IEEE Electron Device Lett, 2014, 35, 69
[69] Kim H R, Yang J H, Kim G H, et al. Flexible vertical-channel thin-film transistors using In-Ga-Zn-O active channel and polyimide spacer on poly(ethylene naphthalate) substrate. J Vac Sci Technol B, 2019, 37, 010602
[70] Liu Y, Zhou H L, Cheng R, et al. Highly flexible electronics from scalable vertical thin film transistors. Nano Lett, 2014, 14, 1413
[71] Yeom H I, Moon G, Nam Y, et al. Oxide vertical TFTs for the application to the ultra high resolution display. SID Symp Dig Tech Pap, 2016, 47, 820
[72] Du P F, Feng P, Wan X, et al. Amorphous $InGaZnO_4$ neuron transistors with temporal and spatial summation function. Chin Phys Lett, 2017, 34, 058502
[73] Kim H E, Furuta M, Yoon S M. A facile doping process of the organic inter-layer dielectric for self-aligned coplanar In-Ga-Zn-O thin-film transistors. IEEE Electron Device Lett, 2020, 41, 393
[74] Zhang Y Q, Yang H, Peng H, et al. Self-aligned top-gate amorphous InGaZnO TFTs with plasma enhanced chemical vapor deposited sub-10 nm SiO_2 gate dielectric for low-voltage applications. IEEE Electron Device Lett, 2019, 40, 1459
[75] Sato A, Abe K, Hayashi R, et al. Amorphous In–Ga–Zn–O coplanar homojunction thin-film transistor. Appl Phys Lett, 2009, 94, 133502
[76] Su L Y, Lin H K, Hung C C, et al. Role ofHfO_2/SiO_2 gate dielectric on the reduction of low-frequent noise and the enhancement of a-IGZO TFT electrical performance. J Disp Technol, 2012, 8, 695
[77] Yamamoto T, Takei T, Nakajima Y, et al. Simple transfer technology for fabrication of TFT backplane for flexible displays. IEEE Trans Ind Appl, 2012, 48, 1662
[78] Hyung G W, Park J, Wang J X, et al. Amorphous indium gallium zinc oxide thin-film transistors with a low-temperature polymeric gate dielectric on a flexible substrate. Jpn J Appl Phys, 2013, 52, 071102
[79] Zhu L Q, Wan C J, Guo L Q, et al. Artificial synapse network on inorganic proton conductor for neuromorphic systems. Nat Commun, 2014, 5, 3158
[80] Yang Y, He Y L, Nie S, et al. Light stimulated IGZO-based electric-double-layer transistors for photoelectric neuromorphic devices. IEEE Electron Device Lett, 2018, 39, 897
[81] Beom K, Yang P, Park D, et al. Single- and double-gate synaptic transistor with TaO_x gate insulator and IGZO channel layer. Nanotechnology, 2019, 30, 025203
[82] Chen T C, Kuo Y, Chang T C, et al. Stability of double gate amorphous In–Ga–Zn–O thin-film transistors with various top gate designs. Jpn J Appl Phys, 2017, 56, 120303
[83] Cho W J, Ahn M J. Bias stress instability of double-gate a-IGZO TFTs on polyimide substrate. J Korean Phys Soc, 2017, 71, 325
[84] He X, Wang L Y, Xiao X, et al. Implementation of fully self-aligned homojunction double-gate a-IGZO TFTs. IEEE Electron Device Lett, 2014, 35, 927
[85] Nathan A, Lee S, Jeon S, et al. Amorphous oxide semiconductor TFTs for displaysand imaging. J Disp Technol, 2014, 10, 917
[86] Kuzum D, Yu S M, Philip Wong H S. Synaptic electronics: Materials, devices and applications. Nanotechnology, 2013, 24, 382001
[87] Mativenga M, Choi M H, Choi J W, et al. Transparent flexible circuits based on amorphous-indium–gallium–zinc–oxide thin-film transistors. IEEE Electron Device Lett, 2011, 32, 170
[88] Cantarella G, Ishida K, Petti L, et al. Flexible In–Ga–Zn–O-based circuits with two and three metal layers: Simulation and fabrication study. IEEE Electron Device Lett, 2016, 37, 1582
[89] Lee S, Jeon S, Chaji R, et al. Transparent semiconducting oxide technology for touch free interactive flexible displays. Proc IEEE, 2015, 103, 644
[90] Hsieh H H, Lu H H, Ting H C, et al. Development of IGZO TFTs and their applications to next-generation flat-panel displays. J Inf Disp, 2010, 11, 160
[91] Baek G, Kanicki J. Modeling of current: Voltage characteristics for double-gate a-IGZO TFTs and its application to AMLCDs. J Soc Inf Display, 2012, 20, 237
[92] Gong N, Park C, Lee J, et al. Implementation of 240Hz 55-inch ultra definition LCD driven by a-IGZO semiconductor TFT with copper signal lines. SID Symp Dig Tech Pap, 2012, 43, 784
[93] Lin C L, Chang W Y, Hung C C. Compensating pixel circuit driving AMOLED display with a-IGZO TFTs. IEEE Electron Device Lett, 2013, 34, 1166
[94] Kim D, Kim Y, Lee S, et al. High resolution a-IGZO TFT pixel circuit for compensating threshold voltage shifts and OLED degradations. IEEE J Electron Devices Soc, 2017, 5, 372
[95] Lai P C, Lin C L, Kanicki J. Novel top-anode OLED/a-IGZO TFTs pixel circuit for 8K4K AM-OLEDs. IEEE Trans Electron Devices, 2019, 66, 436
[96] Liao C, Deng W, Song D, et al. Mirrored OLED pixel circuit for

threshold voltage and mobility compensation with IGZO TFTs. Microelectron J, 2015, 46, 923

[97] Lin C L, Chen F H, Hung C C, et al. New a-IGZO pixel circuit composed of three transistors and one capacitor for use in high-speed-scan AMOLED displays. J Disp Technol, 2015, 11, 1031

[98] Mativenga M, Ha S H, Geng D, et al. Infinite output resistance of corbino thin-film transistors with an amorphous-InGaZnO active layer for large-area AMOLED displays. IEEE Trans Electron Devices, 2014, 61, 3199

[99] Shimazoe K, Koyama A, Takahashi H, et al. Prototype of IGZO-TFT preamplifier and analog counter for pixel detector. J Instrum, 2017, 12, C02045

[100] Shin W S, Ahn H A, Na J S, et al. A driving method of pixel circuit using a-IGZO TFT for suppression of threshold voltage shift in AMLED displays. IEEE Electron Device Lett, 2017, 38, 760

[101] Wang C C, Hu Z J, He X, et al. One gate diode-connected dual-gate a-IGZO TFT driven pixel circuit for active matrix organic light-emitting diode displays. IEEE Trans Electron Devices, 2016, 63, 3800

[102] Yang J Y, Jung S H, Woo C S, et al. A short-channel TFT of amorphous In–Ga–Zn–O semiconductor pixel structure with advanced five-mask process. IEEE Electron Device Lett, 2014, 35, 1043

[103] Zhou L, Xu M, Xia X H, et al. Power consumption model for AMOLED display panel based on 2T-1C pixel circuit. J Display Technol, 2016, 12, 1064

[104] Hara Y, Kikuchi T, Kitagawa H, et al. IGZO-TFT technology for large-screen 8K display. J Soc Inf Disp, 2018, 26, 169

[105] Lin C L, Chen P S, Lai P C, et al. Novel pixel circuit with compensation for normally-off/on a-IGZO TFTs and OLED luminance degradation. J Disp Technol, 2016, 12, 1664

[106] Tai Y H, Chou L S, Chiu H L, et al. Three-transistor AMOLED pixel circuit with threshold voltage compensation function using dual-gate IGZO TFT. IEEE Electron Device Lett, 2012, 33, 393

[107] Jeon C H, Um J G, Mativenga M, et al. Fast threshold voltage compensation AMOLED pixel circuit using secondary gate effect of dual gate a-IGZO TFTs. IEEE Electron Device Lett, 2016, 37, 1450

[108] Bagheri M, Cheng X, Zhang J H, et al. Threshold voltage compensation error in voltage programmed AMOLED displays. J Disp Technol, 2016, 12, 658

[109] Lim W, Jang J H, Kim S H, et al. High performance indium gallium zinc oxide thin film transistors fabricated on polyethylene terephthalate substrates. Appl Phys Lett, 2008, 93, 082102

[110] Fortunato E, Correia N, Barquinha P, et al. High-performance flexible hybrid field-effect transistors based on cellulose fiber paper. IEEE Electron Device Lett, 2008, 29, 988

[111] Lee G J, Kim J, Kim J H, et al. High performance, transparent a-IGZO TFTs on a flexible thin glass substrate. Semicond Sci Technol, 2014, 29, 035003

[112] Münzenrieder N, Zysset C, Petti L, et al. Flexible double gate a-IGZO TFT fabricated on free standing polyimide foil. Solid-State Electron, 2013, 84, 198

[113] Lim W, Douglas E A, Norton D P, et al. Low-voltage indium gallium zinc oxide thin film transistors on paper substrates. Appl Phys Lett, 2010, 96, 053510

[114] Kim Y C, Lee S J, Oh I K, et al. Bending stability of flexible amorphous IGZO thin film transistors with transparent IZO/Ag/IZO oxide-metal-oxide electrodes. J Alloy Compd, 2016, 688, 1108

[115] Munzenrieder N, Cherenack K H, Troster G. The effects of mechanical bending and illumination on the performance of flexible IGZO TFTs. IEEE Trans Electron Devices, 2011, 58, 2041

[116] Nakano S, Saito N, Miura K, et al. Highly reliable a-IGZO TFTs on a plastic substrate for flexible AMOLED displays. J Soc Inf Disp, 2012, 20, 493

[117] Kim J S, Byun J W, Jang J H, et al. A high-reliability carry-free gate driver for flexible displays using a-IGZO TFTs. IEEE Trans Electron Devices, 2018, 65, 3269

[118] Kim D S, Kwon O K. A small-area and low-power scan driver using a coplanar a-IGZO thin-film transistor with a dual-gate for liquid crystal displays. IEEE Electron Device Lett, 2017, 38, 195

[119] Yamaguchi H, Ueda T, Miura K, et al. 11.7-inch flexible AMOLED display driven by a-IGZO TFTs on plastic substrate. SID Symp Dig Tech Pap, 2012, 43, 1002

[120] Yoo W B, Ha C, Kwon J, et al. Flexible a-IGZO TFT for large sized OLED TV. SID Symp Dig Tech Pap, 2018, 49, 714

[121] Zhao Y C, Zhao F, Chang C, et al. The world's first prototype of 85-inch 8K4K 120Hz LCD with BCE-IGZO structure and GOA design. SID Symp Dig Tech Pap, 2018, 49, 330

[122] Kim K M, Han I, Noh S, et al. Bezel free design of organic light emitting diode display via a-InGaZnO gate driver circuit integration within active array. J Soc Inf Disp, 2019, 27, 514

[123] Liu N, Zhu L Q, Feng P, et al. Flexible sensory platform based on oxide-based neuromorphic transistors. Sci Rep, 2015, 5, 18082

[124] Shah S, Smith J, Stowell J, et al. Biosensing platform on a flexible substrate. Sens Actuators B, 2015, 210, 197

[125] Cai G S, Yang P, Wang X Z, et al. Investigation of pH sensor based on liquid-solid dual-gated IGZO thin-film transistor. Mater Res Express, 2019, 6, 096305

[126] Pavlidis S, Getz P, Hagen J, et al. Investigating thin film passivations for IGZO dual gate pH sensors fabrication at low temperature. 2015 18th International Conference on Solid-State Sensors, Actuators and Microsystems, 2015, 1334

[127] Kimura M, Hasegawa T, Ide K, et al. Light irradiation history sensor using amorphous In-Ga-Zn-O thin-film transistor exposed to ozone annealing. IEEE Electron Device Lett, 2012, 33, 384

[128] Liu P T, Ruan D B, Yeh X Y, et al. Highly responsive blue light sensor with amorphous indium-zinc-oxide thin-film transistor based architecture. Sci Rep, 2018, 8, 8153

[129] Pei Z, Lai H C, Wang J Y, et al. High-responsivity and high-sensitivity graphene dots/a-IGZO thin-film phototransistor. IEEE Electron Device Lett, 2015, 36, 44

[130] Yu J, Shin S W, Lee K H, et al. Visible-light phototransistors based on InGaZnO and silver nanoparticles. J Vac Sci Technol B, 2015, 33, 061211

[131] Zan H W, Chen W T, Hsueh H W, et al. Amorphous indium-gallium-zinc-oxide visible-light phototransistor with a polymeric light absorption layer. Appl Phys Lett, 2010, 97, 203506

[132] Tressler J F, Alkoy S, Newnham R E. Piezoelectric sensors and sensor materials. J Electrocera, 1998, 2, 257

[133] Geng D, Han S Y, Seo H, et al. Piezoelectric pressure sensing device using top-gate effect of dual-gate a-IGZO TFT. IEEE Sensor J, 2017, 17, 585

[134] Maity D, Halder S, Roy P. High pH sensing properties of a new schiff-base compound. ChemistrySelect, 2018, 3, 440

[135] Ahn M J, Lim C M, Cho W J. Highly sensitive ion-sensitive field-effect transistor sensor using fully transparent amorphous In–Ga–Zn–O thin-film transistors. Semicond Sci Technol, 2017, 32, 035003

[136] Pyo J Y, Cho W J. High-performance SEGISFET pH Sensor using the structure of double-gate a-IGZO TFTs with engineered gate oxides. Semicond Sci Technol, 2017, 32, 035015

[137] Kim K S, Ahn C H, Jung S H, et al. Toward adequate operation of amorphous oxide thin-film transistors for low-concentration gas detection. ACS Appl Mater Interfaces, 2018, 10, 10185

[138] Lee Y T, Lee J, Hwang H, et al. Novel hydrogen gas sensing by palladium electrode on dielectric capacitor coupled with an amorphous InGaZnO thin-film transistor. Sens Actuators B, 2015, 209, 490

[139] Li B C, Lai P T, Tang W M. Hydrogen sensors based on TFT's with catalytic source/drain electrodes: IGZO vs. pentacene. IEEE Electron Device Lett, 2018, 1

[140] Knobelspies S, Bierer B, Daus A, et al. Photo-induced room-temperature gas sensing with a-IGZO based thin-film transistors fabricated on flexible plastic foil. Sensors, 2018, 18, E358
[141] Tripathi A K, Myny K, Hou B, et al. Electrical characterization of flexible InGaZnO transistors and 8-b transponder chip down to a bending radius of 2 mm. IEEE Trans Electron Devices, 2015, 62, 4063
[142] Chen Y F, Geng D, Lin T D, et al. Full-swing clock generating circuits on plastic using a-IGZO dual-gate TFTs with pseudo-CMOS and bootstrapping. IEEE Electron Device Lett, 2016, 37, 882
[143] Zheng J W, Han S J, Li M M, et al. A full-swing inverter based on IGZO TFTs for flexible circuits. SID Symp Dig Tech Pap, 2018, 49, 709
[144] Bahubalindruni P G, Tiwari B, Pereira M, et al. Rail-to-rail timing signals generation using InGaZnO TFTs for flexible X-ray detector. IEEE J Electron Devices Soc, 2020, 8, 157
[145] Jeon S, Park S, Song I, et al. 180nm gate length amorphous InGaZnO thin film transistor for high density image sensor applications. IEEE International Electron Devices Meeting, 2010
[146] Chang T H, Chiu C J, Chang S J, et al. Amorphous InGaZnO ultraviolet phototransistors with double-stack Ga_2O_3/SiO_2 dielectric. Appl Phys Lett, 2013, 102, 221104
[147] Vijjapu M T, Surya S G, Yuvaraja S, et al. Fully integrated indium gallium zinc oxide NO_2 gas detector. ACS Sens, 2020, 5, 984
[148] Park I J, Jeong C Y, Cho I T, et al. Fabrication of amorphous InGaZnO thin-film transistor-driven flexible thermal and pressure sensors. Semicond Sci Technol, 2012, 27, 105019
[149] Zhang Z H, Chen L L, Yang X, et al. Enhanced flexible piezoelectric sensor by the integration of P(VDF-TrFE)/AgNWs film with a-IGZO TFT. IEEE Electron Device Lett, 2018, 40, 111
[150] Lujan R A, Street R A. Flexible X-ray detector array fabricated with oxide thin-film transistors. IEEE Electron Device Lett, 2012, 33, 688
[151] Machens C K. Building the human brain. Science, 2012, 338, 1156
[152] Merolla P A, Arthur J V, Alvarez-Icaza R, et al. A million spiking-neuron integrated circuit with a scalable communication network and interface. Science, 2014, 345, 668
[153] Zidan M A, Strachan J P, Lu W D. The future of electronics based on memristive systems. Nat Electron, 2018, 1, 22
[154] Xia Q, Yang J J. Memristive crossbar arrays for brain-inspired computing. Nat Mater, 2019, 18, 309
[155] Wang Z R, Li C, Song W H, et al. Reinforcement learning with analogue memristor arrays. Nat Electron, 2019, 2, 115
[156] Tan Z H, Yang R, Terabe K, et al. Synaptic metaplasticity realized in oxide memristive devices. Adv Mater, 2016, 28, 377
[157] Wang J B, Li Y X, Yin C Q, et al. Long-term depression mimicked in an IGZO-based synaptic transistor. IEEE Electron Device Lett, 2017, 38, 191
[158] He Y L, Nie S, Liu R, et al. Indium–gallium–zinc–oxide Schottky synaptic transistors for silent synapse conversion emulation. IEEE Electron Device Lett, 2019, 40, 139
[159] Wan C J, Zhu L Q, Liu Y H, et al. Proton-conducting graphene oxide-coupled neuron transistors for brain-inspired cognitive systems. Adv Mater, 2016, 28, 3557
[160] Wan X, Feng P, Wu G D, et al. Simulation of laterally coupled InGaZnO$_4$-based electric-double-layer transistors for synaptic electronics. IEEE Electron Device Lett, 2015, 36, 204
[161] Zhou J M, Liu N, Zhu L Q, et al. Energy-efficient artificial synapses based on flexible IGZO electric-double-layer transistors. IEEE Electron Device Lett, 2015, 36, 198
[162] Du H W, Lin X, Xu Z M, et al. Electric double-layer transistors: A review of recent progress. J Mater Sci, 2015, 50, 5641
[163] He Y L, Wan Q. Multi-terminal oxide-based electric-double-layer thin-film transistors for neuromorphic systems. ECS Trans, 2018, 86, 177

Ying Zhu received her BS degree in 2018 from the School of Materials Science and Engineering, Nanjing University of Science and Technology, Nanjing, China. Now she is a PhD student at the School of Electronic Science and Engineering, Nanjing University. Her research interests include electric-double-layer synaptic transistors and their application in neuromorphic devices.

Yongli He received his B.S. degree from the School of Physics and Electronics, Hunan University, Changsha, China, in 2016. He is currently a Ph.D candidate at the School of Electronic Science and Engineering, Nanjing University, Nanjing, China. His research interests focus on artificial synaptic and neuronal devices and their application in hardware implementation of neural networks.

Shanshan Jiang got her MD degree from Anhui University in 2018. Now she is a PhD degree student at Nanjing University under the supervision of Prof. Qing Wan. Her research focuses on oxide electric double layer (EDL) thin-film transistor and its application in neuromorphic system.

Qing Wan received his B.S. degree from Zhejiang University, China, in 1998, and Ph.D degree in microelectronics from the Shanghai Institute of Microsystem and Information Technology, Chinese Academy of Sciences, China, in 2004. In 2009, he was awarded "Science and Technology Award for Chinese Youth". Since 2013, he has been a Professor at the School of Electronic Science and Engineering, Nanjing University, China. In 2014, he was supported by the National Science Foundation for Distinguished Young Scholars of China. His research interests focus on: 1) oxide-based thin-film transistors, and 2) neuromorphic devices for brain-like chips.